℘

Inclusive neutrino scattering off the deuteron from threshold to GeV energies

G. Shen,[1,*] L. E. Marcucci,[2,3] J. Carlson,[1] S. Gandolfi,[1] and R. Schiavilla[4,5]

[1]*Theoretical Division, Los Alamos National Laboratory, Los Alamos, New Mexico 87545, USA*
[2]*Department of Physics, University of Pisa, 56127 Pisa, Italy*
[3]*INFN-Pisa, 56127 Pisa, Italy*
[4]*Department of Physics, Old Dominion University, Norfolk, Virginia 23529, USA*
[5]*Jefferson Lab, Newport News, Virginia 23606, USA*

Background: Neutrino-nucleus quasi-elastic scattering is crucial to interpret the neutrino oscillation results in long baseline neutrino experiments. There are rather large uncertainties in the cross section, due to insufficient knowledge on the role of two-body weak currents.

Purpose: Determine the role of two-body weak currents in neutrino-deuteron quasi-elastic scattering up to GeV energies.

Methods: Calculate cross sections for inclusive neutrino scattering off deuteron induced by neutral and charge-changing weak currents, from threshold up to GeV energies, using the Argonne v_{18} potential and consistent nuclear electroweak currents with one- and two-body terms.

Results: Two-body contributions are found to be small, and increase the cross sections obtained with one-body currents by less than 10% over the whole range of energies. Total cross sections obtained by describing the final two-nucleon states with plane waves differ negligibly, for neutrino energies $\gtrsim 500$ MeV, from those in which interaction effects in these states are fully accounted for. The sensitivity of the calculated cross sections to different models for the two-nucleon potential and/or two-body terms in the weak current is found to be weak. Comparing cross sections to those obtained in a naive model in which the deuteron is taken to consist of a free proton and neutron at rest, nuclear structure effects are illustrated to be non-negligible.

Conclusion: Contributions of two-body currents in neutrino-deuteron quasi-elastic scattering up to GeV are found to be smaller than 10%. Finally, it should be stressed that the results reported in this work do not include pion production channels.

I. INTRODUCTION

In the last few years, inclusive neutrino scattering from nuclear targets has become a hot topic. Interest has been spurred by the anomaly observed in recent neutrino quasielastic scattering data on ^{12}C [1,2], i.e., the excess, at relatively low energies, of measured cross sections relative to theoretical calculations. Analyses based on these calculations have led to speculations that our present understanding of the nuclear response to charge-changing weak probes may be incomplete [3], and, in particular, that the momentum transfer dependence of the axial form factor of the nucleon, specifically the cutoff value of its dipole parametrization [4], may be quite different from that obtained from analyses of pion electroproduction data [5] and measurements of the reaction $n(\nu_\mu, \mu^-)p$ in the deuteron at quasielastic kinematics [6,7] and of $\nu_\mu p$ and $\overline{\nu}_\mu p$ elastic scattering [8] ($\Lambda_A \simeq 1.20$ GeV vs. $\Lambda_A \simeq 1$ GeV). However, it should be emphasized that the calculations on which these analyses are based use rather crude models of nuclear structure—Fermi gas or local density approximations of the nuclear matter spectral function—as well as simplistic treatments of the reaction mechanism and should, therefore, be viewed with skepticism.

In this paper, we calculate cross sections for inclusive neutrino scattering off the deuteron over a wide energy range, from threshold up to 1 GeV. The motivations for undertaking such a work are twofold. The first is to provide a benchmark for studies of electroweak inclusive response in light nuclei we intend to carry out in the near-future. The second motivation has to do with plans [9], still under development, to determine the neutrino flux in accelerator-based experiments from measurements of inclusive cross sections on the deuteron. In particular, in charged-current neutrino capture on deuterons, the final states ppl^- can be measured, in principle, very well. Clearly, accurate predictions for these cross sections are crucial for a reliable determination of the flux.

A number of studies of neutrino-deuteron scattering at low and intermediate energies ($\lesssim 150$ MeV) have been carried out in past decades; see Ref. [10] for a review of work done up to the mid 1990s. These efforts culminated in Nakamura *et al.*'s 2001 and 2002 calculations of the cross sections for neutrino disintegration of the deuteron induced by neutral weak currents (NCs) and charge-changing weak currents (CCs). These calculations were based on bound- and scattering-state wave functions obtained from last-generation realistic potentials and used a realistic model for the nuclear weak current, including one- and two-body terms. The vector part of this current was shown to provide an excellent description of the np radiative capture cross section for neutron energies up to 100 MeV [11], while the axial part was constrained

*gshen@uw.edu

to reproduce the Gamow-Teller matrix element in tritium β decay [12]. The Nakamura *et al.* studies have played an important role in the analysis and interpretation of the Sudbury Neutrino Observatory (SNO) experiments [13], which have established solar neutrino oscillations and the validity of the standard model for the generation of energy and neutrinos in the sun [14].

In the present work, we use the same theoretical framework as the authors of Refs. [11,12], but include refinements in the modeling of the weak current—which, however, as shown in Sec. V, will turn out to have a minor impact on the predicted cross sections—and extend the range of neutrino energies up to 1 GeV. While the theoretical approach is essentially the same, the way in which the calculations are carried out in practice is rather different from that used in those earlier papers, which relied on a multipole expansion of the weak transition operators and evaluated the cross section by summing over a relatively large number of final two-nucleon channel states. In contrast, we evaluate, by direct numerical integrations, the matrix elements of the weak current between the deuteron and the two-nucleon scattering states labeled by the relative momentum **p** (and in given pair spin and isospin channels), thus avoiding cumbersome multipole expansions. Differential cross sections are then obtained by integrating over **p** (and summing over the discrete quantum numbers) appropriate combinations of these matrix elements, i.e., by calculating the weak response functions. The techniques developed here for the deuteron should prove valuable when we attempt the Green's function Monte Carlo calculation of these response functions (or, rather, their Laplace transforms [15]) in $A > 2$ nuclei.

This paper is organized as follows. In Sec. II and Appendix A we present the neutrino and antineutrino differential cross sections expressed in terms of response functions, while in Sec. III we provide a succinct description of the NC and CC model. In Sec. IV we outline the methods used to obtain the two-nucleon bound and continuum states and discuss the numerical evaluation of the response functions. A variety of results for the neutral-current processes $^2\mathrm{H}(\nu_l, \nu_l)pn$ and $^2\mathrm{H}(\overline{\nu}_l, \overline{\nu}_l)pn$ and the charge-changing processes $^2\mathrm{H}(\nu_e, e^-)pp$ and $^2\mathrm{H}(\overline{\nu}_e, e^+)nn$ are presented in Sec. V, including the sensitivity of the calculated cross sections to (i) interaction effects in the final states, (ii) different short-range behaviors of the two-body axial weak currents, and (iii) different potential models to describe the two-nucleon bound and continuum states. In order to illustrate the effects of nuclear structure, we compare these cross sections to those obtained in a naive model in which the deuteron is taken to consist of a free proton and neutron (the free nucleon cross sections are listed for reference in Appendix B). Concluding remarks and an outlook are given in Sec. VI.

II. INCLUSIVE NEUTRINO SCATTERING OFF THE DEUTERON

The differential cross section for neutrino (ν) and antineutrino ($\overline{\nu}$) inclusive scattering off the deuteron, specifically the processes

$$\nu_l + d \longrightarrow \nu_l + p + n, \quad \overline{\nu}_l + d \longrightarrow \overline{\nu}_l + p + n, \quad (2.1)$$

induced by NCs, and the processes

$$\nu_l + d \longrightarrow l^- + p + p, \quad \overline{\nu}_l + d \longrightarrow l^+ + n + n, \quad (2.2)$$

induced by CCs, can be expressed as

$$
\left(\frac{d\sigma}{d\epsilon' d\Omega}\right)_{\nu/\overline{\nu}}
$$
$$
= \frac{G^2}{2\pi^2} k' \epsilon' \, F(Z, k') \cos^2\frac{\theta}{2} \left[R_{00} + \frac{\omega^2}{q^2} R_{zz} - \frac{\omega}{q} R_{0z} \right.
$$
$$
\left. + \left(\tan^2\frac{\theta}{2} + \frac{Q^2}{2q^2} \right) R_{xx+yy} \mp \tan\frac{\theta}{2} \sqrt{\tan^2\frac{\theta}{2} + \frac{Q^2}{q^2}} \, R_{xy} \right],
$$
$$(2.3)$$

where $G = G_F$ for NC processes and $G = G_F \cos\theta_C$ for CC processes, and the minus (plus) sign in the last term is relative to the ν ($\overline{\nu}$) initiated reactions. Following Ref. [12], we adopt the value $G_F = 1.1803 \times 10^{-5} \, \mathrm{GeV}^{-2}$ as obtained from an analysis of super-allowed $0^+ \to 0^+$ β decays [16]—this value includes radiative corrections—while $\cos\theta_C$ is taken as 0.97425 from [17]. The initial neutrino four-momentum is $k^\mu = (\epsilon, \mathbf{k})$, the final lepton four-momentum is $k^{\mu'} = (\epsilon', \mathbf{k}')$, and the lepton scattering angle is denoted θ. We have also defined the lepton energy and momentum transfers as $\omega = \epsilon - \epsilon'$ and $\mathbf{q} = \mathbf{k} - \mathbf{k}'$, respectively, and the squared four-momentum transfer as $Q^2 = q^2 - \omega^2 > 0$. The Fermi function $F(Z, k')$ with $Z = 2$ accounts for the Coulomb distortion of the final lepton wave function in the the charge-raising reaction, and is given by

$$
F(Z, k') = 2(1 + \gamma)(2 k' r_d)^{2\gamma - 2} \exp(\pi y) \left| \frac{\Gamma(\gamma + i y)}{\Gamma(1 + 2\gamma)} \right|^2,
$$
$$
\gamma = \sqrt{1 - (Z \alpha)^2}; \quad (2.4)
$$

it is set to 1 otherwise. Here $y = Z \alpha \, \epsilon'/k'$, $\Gamma(z)$ is the gamma function, r_d is the deuteron radius ($r_d = 1.967$ fm), and α is the fine structure constant. Radiative corrections for the CC and NC processes owing to bremsstrahlung and virtual photon and Z exchanges have been evaluated by the authors of Refs. [18,19] at the low energies ($\sim$10 MeV) relevant for the SNO experiment, which measured the neutrino flux from the ^{8}B decay in the sun. These corrections are neglected in the present work, as its focus is on scattering of neutrinos with energies higher than 100 MeV. We are not (or not yet, at least) concerned with providing cross section calculations with percentage accuracy in this regime. Finally, the nuclear response functions are defined as

$$
R_{00}(q, \omega) = \frac{1}{3} \sum_M \sum_f \delta(\omega + m_d - E_f) \langle f | j^0(\mathbf{q}, \omega) | d, M \rangle
$$
$$
\times \langle f | j^0(\mathbf{q}, \omega) | d, M \rangle^*, \quad (2.5)
$$
$$
R_{zz}(q, \omega) = \frac{1}{3} \sum_M \sum_f \delta(\omega + m_d - E_f) \langle f | j^z(\mathbf{q}, \omega) | d, M \rangle
$$
$$
\times \langle f | j^z(\mathbf{q}, \omega) | d, M \rangle^*, \quad (2.6)
$$

$$R_{0z}(q,\omega) = \frac{2}{3} \sum_M \sum_f \delta(\omega + m_d - E_f)$$
$$\times \text{Re}[\langle f|j^0(\mathbf{q},\omega)|d,M\rangle \langle f|j^z(\mathbf{q},\omega)|d,M\rangle^*], \quad (2.7)$$

$$R_{xx+yy}(q,\omega) = \frac{1}{3} \sum_M \sum_f \delta(\omega + m_d - E_f)$$
$$\times [\langle f|j^x(\mathbf{q},\omega)|d,M\rangle \langle f|j^x(\mathbf{q},\omega)|d,M\rangle^*$$
$$+ \langle f|j^y(\mathbf{q},\omega)|d,M\rangle \langle f|j^y(\mathbf{q},\omega)|d,M\rangle^*], \quad (2.8)$$

$$R_{xy}(q,\omega) = \frac{2}{3} \sum_M \sum_f \delta(\omega + m_d - E_f)$$
$$\times \text{Im}[\langle f|j^x(\mathbf{q},\omega)|d,M\rangle \langle f|j^y(\mathbf{q},\omega)|d,M\rangle^*], \quad (2.9)$$

where $|d,M\rangle$ and $|f\rangle$ represent, respectively, the initial deuteron state in spin projection M and the final two-nucleon state of energy E_f, and m_d is the deuteron rest mass. The three-momentum transfer $\mathbf{q}$ is taken along the z axis (i.e., the spin-quantization axis), and $j^\mu(\mathbf{q},\omega)$ is the time component (for $\mu = 0$) or space component (for $\mu = x, y, z$) of the NC or CC.

The expression above for the CC cross section is valid in the limit $\epsilon' \simeq k'$, in which the lepton rest mass is neglected. At a low incident neutrino energy, this approximation is not correct. Inclusion of the lepton rest mass leads to changes in the kinematical factors multiplying the various response functions. The resulting cross section is given in Appendix A.

III. NEUTRAL AND CHARGE-CHANGING WEAK CURRENTS

We denote NCs and CCs as j_{NC}^μ and j_{CC}^μ, respectively. The former is given by

$$j_{\text{NC}}^\mu = -2\sin^2\theta_W \, j_{\gamma,S}^\mu + (1 - 2\sin^2\theta_W) j_{\gamma,z}^\mu + j_z^{\mu 5}, \quad (3.1)$$

where θ_W is the Weinberg angle ($\sin^2\theta_W = 0.2312$ [17]), $j_{\gamma,S}^\mu$ and $j_{\gamma,z}^\mu$ denote, respectively, the isoscalar and isovector pieces of the electromagnetic current, and $j_z^{\mu 5}$ denotes the isovector piece of the axial current (the z on the isovector terms indicates that they transform as the z component of an isovector under rotations in isospin space). Isoscalar contributions to j_{NC}^μ associated with strange quarks are ignored, as experiments at Bates [20] and JLab [21] have found them to be very small.

The CC is written as the sum of polar- and axial-vector components,

$$j_{\text{CC}}^\mu = j_\pm^\mu + j_\pm^{\mu 5}, \quad j_\pm = j_x \pm i j_y. \quad (3.2)$$

The conserved-vector-current (CVC) constraint relates the polar-vector components j_b^μ of the CC to the isovector component $j_{\gamma,z}^\mu$ of the electromagnetic current via

$$[T_a, j_{\gamma,z}^\mu] = i\epsilon_{azb} j_b^\mu, \quad (3.3)$$

where T_a are isospin operators. We now turn to a discussion of the one- and two-body contributions to the NC and CC.

A. One-body terms

The isoscalar components of the one-body electromagnetic current are given by

$$j_{\gamma,S}^0(i) = \left[\frac{G_E^S(Q^2)}{2\sqrt{1+Q^2/(4m^2)}} \right.$$
$$\left. - i\frac{2G_M^S(Q^2) - G_E^S(Q^2)}{8m^2} \mathbf{q}\cdot(\boldsymbol{\sigma}_i \times \mathbf{p}_i) \right] e^{i\mathbf{q}\cdot\mathbf{r}_i}, \quad (3.4)$$

$$\mathbf{j}_{\gamma,S}^\perp(i) = \left[\frac{G_E^S(Q^2)}{2m} \mathbf{p}_i^\perp - i\frac{G_M^S(Q^2)}{4m} \mathbf{q}\times\boldsymbol{\sigma}_i \right] e^{i\mathbf{q}\cdot\mathbf{r}_i}, \quad (3.5)$$

$$j_{\gamma,S}^\parallel(i) = j_{\gamma,S}^0(i)\,\omega/q, \quad (3.6)$$

and the corresponding isovector components of $j_{\gamma,z}^\mu$ are obtained by the replacements

$$G_E^S(Q^2) \longrightarrow G_E^V(Q^2)\,\tau_{i,z}, \quad G_M^S(Q^2) \longrightarrow G_M^V(Q^2)\,\tau_{i,z}, \quad (3.7)$$

where $G_E^{S/V}$ and $G_M^{S/V}$ are the isoscalar/isovector combinations of the proton and neutron electric (E) and magnetic (M) form factors, $\mathbf{r}_i$ and $\mathbf{p}_i$ are the position and momentum operators of nucleon i, $\boldsymbol{\sigma}_i$ and $\tau_{i,z}$ are its Pauli spin and isospin matrices, and m is the nucleon mass (0.9389 GeV). Note that we have decomposed $\mathbf{j}_{\gamma,S}$ and $\mathbf{j}_{\gamma,z}$ into transverse ($\perp$) and longitudinal ($\parallel$) components to the momentum transfer $\mathbf{q}$ and have used current conservation to relate the latter to the isoscalar and isovector charge operators $j_{\gamma,S}^0$ and $j_{\gamma,z}^0$. The isovector components of the axial weak neutral current $j_z^{\mu 5}$ are given by

$$j_z^{05}(i) = -\frac{G_A(Q^2)}{4m}\tau_{i,z}\,\boldsymbol{\sigma}_i\cdot[\mathbf{p}_i, e^{i\mathbf{q}\cdot\mathbf{r}_i}]_+, \quad (3.8)$$

$$\mathbf{j}_z^5(i) = -\frac{G_A(Q^2)}{2}\tau_{i,z}\left[\boldsymbol{\sigma}_i e^{i\mathbf{q}\cdot\mathbf{r}_i} - \frac{1}{4m^2}\left(\boldsymbol{\sigma}_i [\mathbf{p}_i^2, e^{i\mathbf{q}\cdot\mathbf{r}_i}]_+ \right.\right.$$
$$- [(\boldsymbol{\sigma}_i\cdot\mathbf{p}_i)\mathbf{p}_i, e^{i\mathbf{q}\cdot\mathbf{r}_i}]_+ - \frac{1}{2}\boldsymbol{\sigma}_i\cdot\mathbf{q}\,[\mathbf{p}_i, e^{i\mathbf{q}\cdot\mathbf{r}_i}]_+$$
$$\left.\left. - \frac{1}{2}\mathbf{q}\,[\boldsymbol{\sigma}_i\cdot\mathbf{p}_i, e^{i\mathbf{q}\cdot\mathbf{r}_i}]_+ + i\,\mathbf{q}\times\mathbf{p}_i\, e^{i\mathbf{q}\cdot\mathbf{r}_i} \right) \right], \quad (3.9)$$

where G_A is the nucleon axial form factor, and $[\ldots,\ldots]_+$ denotes the anticommutator. The operators above include terms of order $(v/c)^2$ in the nonrelativistic expansion of the single-nucleon covariant currents. These have been neglected in Ref. [12]. The proton and neutron electromagnetic and nucleon axial form factors are parametrized as

$$G_E^p(Q^2) = G_D(Q^2), \quad G_E^n(Q^2) = -\mu_n\frac{Q^2}{4m^2}\frac{G_D(Q^2)}{1+Q^2/m^2}, \quad (3.10)$$

$$G_M^p(Q^2) = \mu_p\,G_D(Q^2), \quad G_M^n(Q^2) = \mu_n\,G_D(Q^2), \quad (3.11)$$

$$G_D(Q^2) = \frac{1}{(1+Q^2/\Lambda^2)^2}, \quad G_A(Q^2) = \frac{g_A}{(1+Q^2/\Lambda_A^2)^2}, \quad (3.12)$$

from which the isoscalar and isovector combinations are obtained as $G_{E,M}^{S/V} = G_{E,M}^p \pm G_{E,M}^n$. The proton and neutron

magnetic moments are $\mu_p = 2.793$ and $\mu_n = -1.913$ in units of nuclear magnetons (n.m.), and the nucleon axial-vector coupling constant is taken to be $g_A = 1.2694$ [17]. The values for the cutoff masses Λ and Λ_A used in this work are 0.833 and 1 GeV, respectively. The former is from fits to elastic electron scattering data off the proton and deuteron [22], while the latter is from an analysis of pion electroproduction [5] and neutrino scattering [6–8] data. Uncertainties in the Q^2 dependence of the axial form factor, in particular, the value of Λ_A, could significantly impact predictions for the neutrino cross sections under consideration. As mentioned earlier, recent analyses of neutrino quasielastic scattering data on nuclear targets [4] quote considerably larger values for Λ_A, in the range (1.20–1.35) GeV.

The polar-vector ($j_\pm^\mu$) and axial-vector ($j_\pm^{\mu 5}$) components of the CC are obtained, respectively, from $j_{\gamma,z}^\mu$ and $j_z^{\mu 5}$ by replacing

$$\tau_{i,z}/2 \longrightarrow \tau_{i,\pm} = (\tau_{i,x} \pm \tau_{i,y})/2. \quad (3.13)$$

However, in the case of $j_\pm^{\mu 5}$, in addition to the terms entering Eqs. (3.8) and (3.9), we also retain the induced pseudoscalar contribution, given by

$$j_\pm^{\mu 5}(i; \text{PS}) = -\frac{G_{\text{PS}}(Q^2)}{2\,m\,m_\mu}\,\tau_{i,\pm}\,q^\mu\,\boldsymbol{\sigma}_i \cdot \mathbf{q}\,e^{i\mathbf{q}\cdot\mathbf{r}_i}, \quad (3.14)$$

where the induced pseudoscalar form factor G_{PS} is parametrized as

$$G_{\text{PS}}(Q^2) = -\frac{2\,m_\mu\,m}{m_\pi^2 + Q^2}\,G_A(Q^2). \quad (3.15)$$

This form factor is not well known [23]. The parametrization above is consistent with values extracted [24,25] from precise measurements of muon-capture rates on hydrogen [26] and ^{3}He [27], as well as with the most recent theoretical predictions based on chiral perturbation theory [28]. This contribution vanishes in NC-induced neutrino reactions.

B. Two-body terms

Two-body terms in NCs and CCs have been discussed in considerable detail in Refs. [29–31] (and references therein). We list the terms included in the present study—i.e., the subset of those derived in the above references expected to give the dominant two-body contributions to the processes of interest here—in the following two subsections for clarity of presentation and future reference in Sec. V. Unless stated otherwise, they are given in momentum space, and configuration-space expressions follow from

$$O(\mathbf{q}) = \int_{\mathbf{k}_i}\int_{\mathbf{K}_i}\int_{\mathbf{k}_j}\int_{\mathbf{K}_j} (2\pi)^3\,\delta(\mathbf{k}_i + \mathbf{k}_j - \mathbf{q})\,e^{i\,\mathbf{k}_i\cdot(\mathbf{r}_i' + \mathbf{r}_i)/2}$$
$$\times e^{i\,\mathbf{K}_i\cdot(\mathbf{r}_i' - \mathbf{r}_i)}e^{i\,\mathbf{k}_j\cdot(\mathbf{r}_j' + \mathbf{r}_j)/2}e^{i\,\mathbf{K}_j\cdot(\mathbf{r}_j' - \mathbf{r}_j)}O(\mathbf{k}_i, \mathbf{K}_i, \mathbf{k}_j, \mathbf{K}_j), \quad (3.16)$$

where $\mathbf{k}_i = \mathbf{p}_i' - \mathbf{p}_i$ and $\mathbf{K}_i = (\mathbf{p}_i' + \mathbf{p}_i)/2$, $\mathbf{p}_i$ and $\mathbf{p}_i'$ are the initial and final momenta of nucleon i, and

$$\int_{\mathbf{p}} \equiv \int \frac{d\mathbf{p}}{(2\pi)^3}. \quad (3.17)$$

These configuration-space operators are used in the calculations reported below.

1. Two-body vector terms

The two-body isovector current operator $\mathbf{j}_{\gamma,z}(ij)$ consists of pseudoscalar- and vector-meson (referred to as π-like and ρ-like) exchange and Δ-excitation terms,

$$\mathbf{j}_{\gamma,z}(ij) = \sum_{c=\pi,\,\rho,\,\Delta} [\mathbf{j}_{\gamma,z}(ij; c) + i \rightleftharpoons j]. \quad (3.18)$$

The π-like and ρ-like exchange currents read

$$\mathbf{j}_{\gamma,z}(ij; \pi) = i\,G_E^V(Q^2)(\boldsymbol{\tau}_i \times \boldsymbol{\tau}_j)_z\,v_\pi(k_j)$$
$$\times \left[\boldsymbol{\sigma}_i - \frac{\mathbf{k}_i - \mathbf{k}_j}{k_i^2 - k_j^2}\,(\boldsymbol{\sigma}_i \cdot \mathbf{k}_i)\right]\boldsymbol{\sigma}_j \cdot \mathbf{k}_j, \quad (3.19)$$

$$\mathbf{j}_{\gamma,z}(ij; \rho) = -i\,G_E^V(Q^2)(\boldsymbol{\tau}_i \times \boldsymbol{\tau}_j)_z\Big[v_\rho(k_j)\,\boldsymbol{\sigma}_i \times (\boldsymbol{\sigma}_j \times \mathbf{k}_j)$$
$$+ \frac{v_\rho(k_j)}{k_i^2 - k_j^2}[(\mathbf{k}_i - \mathbf{k}_j)(\boldsymbol{\sigma}_i \times \mathbf{k}_i) \cdot (\boldsymbol{\sigma}_j \times \mathbf{k}_j)$$
$$+ (\boldsymbol{\sigma}_i \times \mathbf{k}_i)\,\boldsymbol{\sigma}_j \cdot (\mathbf{k}_i \times \mathbf{k}_j)$$
$$+ (\boldsymbol{\sigma}_j \times \mathbf{k}_j)\,\boldsymbol{\sigma}_i \cdot (\mathbf{k}_i \times \mathbf{k}_j)]$$
$$- v_{\rho S}(k_j)\frac{\mathbf{k}_i - \mathbf{k}_j}{k_i^2 - k_j^2}\Big], \quad (3.20)$$

where

$$v_\pi(k) = v^{\sigma\tau}(k) - 2\,v^{t\tau}(k), \quad v_\rho(k) = v^{\sigma\tau}(k) + v^{t\tau}(k),$$
$$v_{\rho S}(k) = v^\tau(k), \quad (3.21)$$

and

$$v^\tau(k) = 4\pi \int_0^\infty r^2 dr\,j_0(kr)v^\tau(r), \quad (3.22)$$

$$v^{\sigma\tau}(k) = \frac{4\pi}{k^2}\int_0^\infty r^2 dr\,[j_0(kr) - 1]\,v^{\sigma\tau}(r), \quad (3.23)$$

$$v^{t\tau}(k) = \frac{4\pi}{k^2}\int_0^\infty r^2 dr\,j_2(kr)v^{t\tau}(r). \quad (3.24)$$

Here $v^\tau(r)$, $v^{\sigma\tau}(r)$, and $v^{t\tau}(r)$ are the isospin-dependent central, spin-spin, and tensor components of the two-nucleon interaction (the AV18 in the present study), and $j_l(kr)$ are spherical Bessel functions. The factor $j_0(kr) - 1$ in the expression for $v^{\sigma\tau}(k)$ ensures that its volume integral vanishes. In a one-boson-exchange (OBE) model, in which the isospin-dependent central, spin-spin, and tensor interactions are caused by π- and ρ-meson exchange, the functions $v_\pi(k)$, $v_\rho(k)$, and $v_{\rho S}(k)$ simply reduce to

$$v_\pi(k) \longrightarrow -\frac{f_\pi^2}{m_\pi^2}\frac{h_\pi^2(k)}{k^2 + m_\pi^2}, \quad (3.25)$$

$$v_\rho(k) \longrightarrow -\frac{g_\rho^2(1 + k_\rho)^2}{4\,m^2}\frac{h_\rho^2(k)}{k^2 + m_\rho^2}, \quad (3.26)$$

$$v_{\rho S}(k) \longrightarrow g_\rho^2 \frac{h_\rho^2(k)}{k^2 + m_\rho^2}, \qquad (3.27)$$

where m_π and m_ρ are the meson masses, f_π, g_ρ and κ_ρ are the pseudovector πNN, and vector and tensor ρNN coupling constants, and the hadronic form factors are parameterized as

$$h_\alpha(k) = \frac{\Lambda_\alpha^2 - m_\alpha^2}{\Lambda_\alpha^2 + k^2}, \quad \alpha = \pi, \rho. \qquad (3.28)$$

While the AV18 interaction is not an OBE model, the effective propagators $v_\pi(k)$, $v_\rho(k)$, and $v_{\rho S}(k)$ projected out of its $v^\tau(k)$, $v^{\sigma\tau}(k)$, and $v^{t\tau}(k)$ components are quite similar to those listed above, with cutoff masses in the range (1.0–1.5) GeV. We note that the π-like and ρ-like currents with the $v_\pi(k)$, $v_\rho(k)$, and $v_{\rho S}(k)$ defined in Eq. (3.21) satisfy by construction the current conservation relation with the AV18 τ, $\sigma\tau$, and $t\tau$ interaction components (for a discussion of the issue of current conservation in relation to the momentum-dependent terms of the AV18, see Ref. [31]).

The isovector Δ-excitation current is written in configuration space as (for a derivation based on a perturbative treatment of Δ-isobar degrees of freedom in nuclear wave functions, see Ref. [29])

$$\mathbf{j}_{\gamma,z}(ij; \Delta) = -i \frac{G_{\gamma N\Delta}(Q^2)}{2 m (m - m_\Delta)} e^{i\mathbf{q}\cdot\mathbf{r}_i}$$
$$\times [v_{\Delta N}^\dagger(ij)\, \mathbf{q} \times \mathbf{S}_i\, T_{i,z} + \text{adjoint}], \quad (3.29)$$

where $\mathbf{S}$ and $\mathbf{T}$ are spin- and isospin-transition operators converting a nucleon into a Δ isobar and satisfying the identity

$$\mathbf{S}^\dagger \cdot \mathbf{A}\, \mathbf{S} \cdot \mathbf{B} = \frac{2}{3} \mathbf{A} \cdot \mathbf{B} - \frac{i}{3} \boldsymbol{\sigma} \cdot (\mathbf{A} \times \mathbf{B}), \qquad (3.30)$$

$v_{\Delta N}(ij)$ is the NN-to-ΔN transition potential,

$$v_{\Delta N}(ij) = \left[v_{\Delta N}^{\sigma\tau}(r_{ij}) \mathbf{S}_i \cdot \boldsymbol{\sigma}_j + v_{\Delta N}^{t\tau}(r_{ij}) S_{ij}^{\Delta N} \right] \mathbf{T}_i \cdot \boldsymbol{\tau}_j, \quad (3.31)$$

$S_{ij}^{\Delta N}$ is the tensor operator obtained by replacing $\boldsymbol{\sigma}_i$ with $\mathbf{S}_i$, the regularized spin-spin and tensor radial functions $v_{\Delta N}^{\sigma\tau}(r)$ and $v_{\Delta N}^{t\tau}(r)$ are defined as

$$v_{\Delta N}^{\sigma\tau}(r) = \frac{f_\pi f_\pi^*}{4\pi} \frac{m_\pi}{3} \frac{e^{-x}}{x} \left(1 - e^{-\lambda x^2}\right), \qquad (3.32)$$

$$v_{\Delta N}^{t\tau}(r) = \frac{f_\pi f_\pi^*}{4\pi} \frac{m_\pi}{3} \left(1 + \frac{3}{x} + \frac{3}{x^2}\right) \frac{e^{-x}}{x} \left(1 - e^{-\lambda x^2}\right)^2, \quad (3.33)$$

$x = m_\pi r$, f_π^* is the $\pi N\Delta$ coupling constant ($f_\pi^* = 2.19 f_\pi$ from the width of the Δ), and the parameter in the short-range cutoff function is taken as $\lambda = 4.29$ (from the AV18). Finally, the $\gamma N\Delta$ electromagnetic transition form factor $G_{\gamma N\Delta}$ is parameterized as

$$G_{\gamma N\Delta}(Q^2) = \frac{\mu_{\gamma N\Delta}}{\left(1 + Q^2/\Lambda_{\Delta,1}^2\right)^2 \sqrt{1 + Q^2/\Lambda_{\Delta,2}^2}}, \quad (3.34)$$

where the transition magnetic moment $\mu_{\gamma N\Delta}$ is 3 n.m., as obtained in an analysis of γN data in the Δ-resonance region [32]. This analysis also gives $\Lambda_{\Delta,1} = 0.84$ GeV and $\Lambda_{\Delta,2} = 1.2$ GeV.

The two-body isoscalar current operator $\mathbf{j}_{\gamma,S}(ij)$ considered in the present study only includes the contribution associated with the $\rho\pi\gamma$ transition mechanism,

$$\mathbf{j}_{\gamma,S}(ij) = \mathbf{j}_{\gamma,S}(ij; \rho\pi) + i \rightleftharpoons j, \qquad (3.35)$$

where

$$\mathbf{j}_{\gamma,S}(ij; \rho\pi) = -i\, G_{\rho\pi\gamma}(Q^2)\, g_{\rho\pi\gamma} \frac{f_\pi}{m_\pi} \frac{g_\rho}{m_\rho}\, \boldsymbol{\tau}_i \cdot \boldsymbol{\tau}_j \frac{h_\rho(k_i)}{k_i^2 + m_\rho^2}$$
$$\times \frac{h_\pi(k_j)}{k_j^2 + m_\pi^2} (\mathbf{k}_i \times \mathbf{k}_j)\, \boldsymbol{\sigma}_j \cdot \mathbf{k}_j, \qquad (3.36)$$

The combination of coupling constants $g_{\rho\pi\gamma} f_\pi g_\rho$ is taken as 1.37, and the cutoff masses Λ_π and Λ_ρ as 0.75 and 1.25 GeV, respectively, from a study of the deuteron magnetic form factor [33]. The Q^2 dependence of the electromagnetic transition form factor $G_{\rho\pi\gamma}(Q^2)$ is modeled by using vector-meson dominance,

$$G_{\rho\pi\gamma}(Q^2) = \frac{1}{1 + Q^2/m_\omega^2}, \qquad (3.37)$$

where m_ω is the ω-meson mass.

The two-body isovector and isoscalar electromagnetic charge operators $j_{\gamma,z}^0$ and $j_{\gamma,S}^0$ consist of terms associated with π-like and ρ-like exchanges,

$$j_{\gamma,z/S}^0(ij) = \sum_{c=\pi, \rho} \left[j_{\gamma,z/S}^0(ij; c) + i \rightleftharpoons j \right], \quad (3.38)$$

where

$$j_{\gamma,z}^0(ij; \pi) = \frac{F_1^V(Q^2)}{2 m} \tau_{z,j}\, v_\pi(k_j) (\boldsymbol{\sigma}_i \cdot \mathbf{q})(\boldsymbol{\sigma}_j \cdot \mathbf{k}_j), \quad (3.39)$$

$$j_{\gamma,z}^0(ij; \rho) = \frac{F_1^V(Q^2)}{2 m} \tau_{z,j}\, v_\rho(k_j) (\boldsymbol{\sigma}_i \times \mathbf{q}) \cdot (\boldsymbol{\sigma}_j \times \mathbf{k}_j) \quad (3.40)$$

and

$$j_{\gamma,S}^0(ij; \pi) = \frac{F_1^S(Q^2)}{2 m} \boldsymbol{\tau}_i \cdot \boldsymbol{\tau}_j\, v_\pi(k_j) (\boldsymbol{\sigma}_i \cdot \mathbf{q})(\boldsymbol{\sigma}_j \cdot \mathbf{k}_j), \qquad (3.41)$$

$$j_{\gamma,S}^0(ij; \rho) = \frac{F_1^S(Q^2)}{2 m} \boldsymbol{\tau}_i \cdot \boldsymbol{\tau}_j\, v_\rho(k_j) (\boldsymbol{\sigma}_i \times \mathbf{q}) \cdot (\boldsymbol{\sigma}_j \times \mathbf{k}_j), \qquad (3.42)$$

with $v_\pi(k)$ and $v_\rho(k)$ as defined in Eqs. (3.21). The nucleon electromagnetic Dirac and Pauli form factors $F_1^{S/V}$ and $F_2^{S/V}$ are obtained from

$$F_1^{S/V}(Q^2) = \frac{G_E^{S/V}(Q^2) + \eta\, G_M^{S/V}(Q^2)}{1 + \eta}, \qquad (3.43)$$

$$F_2^{S/V}(Q^2) = \frac{G_M^{S/V}(Q^2) - G_E^{S/V}(Q^2)}{1 + \eta}, \qquad (3.44)$$

with $\eta = Q^2/(4 m^2)$.

The polar-vector components $j_\pm^\mu$ of the CC j_{CC}^μ are obtained from $j_{\gamma,z}^\mu$ via CVC, which implies the replacements

$$(\boldsymbol{\tau}_i \times \boldsymbol{\tau}_j)_z \longrightarrow (\boldsymbol{\tau}_i \times \boldsymbol{\tau}_j)_\pm = (\boldsymbol{\tau}_i \times \boldsymbol{\tau}_j)_x \pm i\, (\boldsymbol{\tau}_i \times \boldsymbol{\tau}_j)_y$$
$$(3.45)$$

in Eqs. (3.19) and (3.20),

$$T_{i,z}/2 \longrightarrow T_{i,\pm} = (T_{i,x} \pm i\, T_{i,y})/2 \qquad (3.46)$$

in Eq. (3.29), and the replacement (3.13) in Eqs. (3.39) and (3.40). Only the transverse components (perpendicular to **q**) of the vector part of the NC and CC are explicitly included in the calculations to follow. Their longitudinal components have already been effectively accounted for by the replacement in Eq. (3.6) (and the similar one for the isovector terms). Finally, we note that in the study in Ref. [12] the ρ-meson exchange and $\rho\pi$ transition contributions to the two-body vector current and π- and ρ-exchange contributions to the two-body vector charge have been neglected. Furthermore, the π-exchange and Δ-excitation currents are regularized by introducing a monopole form factor ($\Lambda_\pi = 4.8 \, \text{fm}^{-1}$), which naturally leads to a short-range behavior of these currents different from that obtained here.

2. Two-body axial terms

The axial parts of NC and CC operators consist of contributions associated with π- and ρ-meson exchanges, the axial $\rho\pi$ transition mechanism, and a Δ-excitation term

$$\mathbf{j}_a^5(ij) = \sum_{c=\pi,\,\rho,\,\rho\pi,\,\Delta} \left[\mathbf{j}_a^5(ij;c) + i \rightleftharpoons j \right], \quad (3.47)$$

where the isospin component a is either z for NC or $\pm$ for CC. The π- and ρ-meson exchange and $\rho\pi$ transition axial currents read, respectively,

$$\mathbf{j}_z^5(ij;\pi) = \frac{G_A(Q^2)}{2\,m} \frac{f_\pi^2}{m_\pi^2} \frac{h_\pi^2(k_j)}{k_j^2 + m_\pi^2} [(\boldsymbol{\tau}_i \times \boldsymbol{\tau}_j)_z \, \boldsymbol{\sigma}_i \times \mathbf{k}_j$$
$$- \tau_{j,z}(\mathbf{q} + 2\,i\,\boldsymbol{\sigma}_i \times \mathbf{K}_i)] \, \boldsymbol{\sigma}_j \cdot \mathbf{k}_j, \quad (3.48)$$

$$\mathbf{j}_z^5(ij;\rho) = -\frac{G_A(Q^2)}{2\,m} \frac{g_\rho^2 (1+k_\rho)^2}{4\,m^2} \frac{h_\rho^2(k_j)}{k_j^2 + m_\rho^2} [(\boldsymbol{\tau}_i \times \boldsymbol{\tau}_j)_z$$
$$\times [\mathbf{q}\,\boldsymbol{\sigma}_i \cdot (\boldsymbol{\sigma}_j \times \mathbf{k}_j) + 2\,i\,(\boldsymbol{\sigma}_j \times \mathbf{k}_j) \times \mathbf{K}_i$$
$$- [\boldsymbol{\sigma}_i \times (\boldsymbol{\sigma}_j \times \mathbf{k}_j)] \times \mathbf{k}_j]$$
$$+ \tau_{j,z}[(\boldsymbol{\sigma}_j \times \mathbf{k}_j) \times \mathbf{k}_j$$
$$- 2\,i[\boldsymbol{\sigma}_i \times (\boldsymbol{\sigma}_j \times \mathbf{k}_j)] \times \mathbf{K}_i]], \quad (3.49)$$

$$\mathbf{j}_z^5(ij;\rho\pi) = -\frac{G_A(Q^2)}{m} g_\rho^2 \frac{h_\rho(k_i)}{k_i^2 + m_\rho^2} \frac{h_\pi(k_j)}{k_j^2 + m_\pi^2} (\boldsymbol{\tau}_i \times \boldsymbol{\tau}_j)_z$$
$$\times [(1+\kappa_\rho)\,\boldsymbol{\sigma}_i \times \mathbf{k}_i - 2\,i\,\mathbf{K}_i] \, \boldsymbol{\sigma}_j \cdot \mathbf{k}_j, \quad (3.50)$$

while the Δ-excitation axial current is obtained from [29]

$$\mathbf{j}_z^5(ij;\Delta) = -\frac{G_A^*(Q^2)}{2\,(m - m_\Delta)} e^{i\mathbf{q}\cdot\mathbf{r}_i}[v_{\Delta N}^\dagger(ij)\,\mathbf{S}_i\,T_{i,z} + \text{adjoint}],$$
$$(3.51)$$

where the (unknown) N-to-Δ axial form factor is parameterized as

$$G_A^*(Q^2) = \frac{g_A^*}{\left(1 + Q^2/\Lambda_A^2\right)^2}. \quad (3.52)$$

The charge-changing axial currents follow by replacing the isospin operators as in Eqs. (3.13), (3.45) and (3.46). The values for the π- and ρ-meson coupling constants are taken from the CD-Bonn OBE model [34], $f_\pi^2/(4\pi) = 0.075$, $g_\rho^2/(4\pi) = 0.84$, and $\kappa_\rho = 6.1$, while two different sets of

TABLE I. Contributions to the Gamow-Teller matrix element in tritium β decay. The one-body (1-b) non-relativistic (NR) and relativistic correction (RC) contributions are, respectively, from the leading and $1/m^2$ terms in Eq. (3.9); the two-body (2-b) contributions are from Eqs. (3.48)–(3.51). Set I (II) corresponds to the cutoff choices $\Lambda_\pi = \Lambda_\rho = 1.2$ GeV ($\Lambda_\pi = 1.72$ GeV and $\Lambda_\rho = 1.31$ GeV). The N-to-Δ axial coupling constant g_A^* for each set is obtained by fitting the experimental value of the Gamow-Teller matrix element, given by 0.955 ± 0.002 [25].

	Set I	Set II
1-b		
NR	+0.9213	+0.9213
RC	−0.0085	−0.0085
2-b		
π	+0.0078	+0.0123
ρ	−0.0042	−0.0055
$\rho\pi$	+0.0123	+0.0196
Δ	+0.0263	+0.0159
g_A^*/g_A	0.614	0.371

cutoff masses Λ_π and Λ_ρ are used in the present work: $\Lambda_\pi = \Lambda_\rho = 1.2$ GeV (set I), in line with the cutoff masses extracted from the π-like and ρ-like exchanges associated with the AV18 model; and $\Lambda_\pi = 1.72$ GeV and $\Lambda_\rho = 1.31$ GeV (set II) from the CD-Bonn model. In the N-to-Δ axial current, the Q^2 dependence of the form factor is taken to be the same as that of the nucleon; however, the value for the transition axial coupling constant g_A^* is determined by fitting the Gamow-Teller matrix element of tritium β decay [25] in a calculation based on trinucleon wave functions corresponding to the AV18/UIX Hamiltonian and the present model for the axial current. The values corresponding to sets I and II of cutoff masses are listed in Table I.

Finally, in the present study the axial charge operator is taken to include only the pion-exchange term, whose structure and strength are determined by soft-pion theorem and current algebra arguments [35]

$$j_a^{05}(ij) = j_a^{05}(ij;\pi) + i \rightleftharpoons j, \quad (3.53)$$

where

$$j_a^{05}(ij;\pi) = -i\,\frac{G_A(Q^2)}{4\,F_\pi^2} \frac{h_\pi^2(k_i)}{k_i^2 + m_\pi^2} (\boldsymbol{\tau}_i \times \boldsymbol{\tau}_j)_a \, \boldsymbol{\sigma}_i \cdot \mathbf{k}_i, \quad (3.54)$$

F_π is pion-decay amplitude ($F_\pi = 93$ MeV), and the Q^2 dependence of the associated form factor is assumed to be the same as in the nucleon. We conclude by noting that the model described above for the two-body axial charge and current operators is essentially the same as that used in Ref. [12], apart from differences in the values of the cutoff masses for the hadronic form factors of the meson-exchange terms and a different treatment of the Δ-excitation current. However, it is important to stress that both here and in Ref. [12] the two-body axial currents are constrained to reproduce the experimental tritium β-decay rate.

IV. CALCULATION

The two-body scattering- and bound-state problems are solved in momentum space with the methods discussed in Ref. [36], which facilitates calculations with a nonlocal potential such as CD-Bonn. We briefly summarize them in the next two subsections for clarity. In the last subsection we discuss the calculation of the weak-current matrix elements, response functions, and cross sections.

A. The scattering-state problem in momentum space

In the case of scattering (setting aside the treatment of the Coulomb interaction for the time being), we solve for the K matrix in channel JST [hereafter, L is the relative orbital angular momentum, S and T are the total spin and isospin, and J is the total angular momentum, and $(-1)^{L+S+T} = -1$],

$$K_{L'L}^{JST}(p';p) = v_{L'L}^{JST}(p';p) + \frac{4\mu}{\pi}\int_0^\infty dk\, k^2$$
$$\times \sum_{L''} v_{L'L''}^{JST}(p';k)\frac{\mathcal{P}}{p^2-k^2}K_{L''L}^{JST}(k;p), \quad (4.1)$$

where μ is the two-nucleon reduced mass, $\mathcal{P}$ denotes a principal-value integration, and $v_{L'L}^{JST}(p',p)$ are the p-space matrix elements of the potential, projected in channel JST [36]. We should note the presence of the somewhat unconventional phase factor $i^{L-L'}$ included in the matrix elements $v_{L'L}^{JST}(p';p)$ [36], which makes the states used here differ by a factor i^L from those usually adopted in nucleon-nucleon scattering analyses. The integral equations (4.1) are discretized, and the resulting systems of linear equations are solved by direct numerical inversion. The principal-value integration is eliminated by a standard subtraction technique [37]. Phase shifts in channel JST are easily obtained from the on-shell S matrix related to the (on-shell) K matrix by

$$S^{JST}(p) = [1 + 2i\,\mu\,p\,K^{JST}(p;p)]^{-1}$$
$$\times [1 - 2i\,\mu\,p\,K^{JST}(p;p)], \quad (4.2)$$

while r-space wave functions follow from

$$z_{L'L}^{JST}(r;p)$$
$$= \left[j(pr) + \frac{4\mu}{\pi}\int_0^\infty dk\, k^2\, j(kr)\frac{\mathcal{P}}{p^2-k^2}K^{JST}(k;p)\right]_{L'L''}$$
$$\times [1 + 2i\,\mu\,p\,K^{JST}(p;p)]_{L''L}^{-1}, \quad (4.3)$$

where the matrix $[j(pr)]_{L'L} \equiv \delta_{L'L}\, j_L(pr)$ has been introduced for convenience. The (complex) radial wave functions $z_{L'L}^{JST}(r)$ behave in the asymptotic region $r \to \infty$ as

$$z_{L'L}^{JST}(r;p) \simeq \tfrac{1}{2}\big[\delta_{L'L}h_L^{(2)}(pr) + h_{L'}^{(1)}(pr)S_{L'L}^{JST}(p)\big], \quad (4.4)$$

where the functions $h_L^{(1,2)}(pr)$ are defined in terms of the regular and irregular (n_L) spherical Bessel functions as

$$h_L^{(1,2)}(y) = j_L(y) \pm i\, n_L(y). \quad (4.5)$$

In the calculation of the response functions that follows, scattering wave functions with incoming-wave boundary

condition $(-)$ are required. These are written as

$$\psi_{SM_S,TM_T}^{(-)}(\mathbf{r};\mathbf{p}) = 4\pi\sqrt{2}\sum_{JM_J,J\leqslant J_{max}}\sum_{LL'}i^{L'}Z_{LSM_S}^{JM_J*}(\hat{\mathbf{p}})$$
$$\times \big[z_{L'L}^{JST*}(r;p) - \delta_{L'L}\,j_L(pr)\big]\mathcal{Y}_{L'SJ}^{M_J}(\hat{\mathbf{r}})\,\eta_{M_T}^T$$
$$+ \frac{1}{\sqrt{2}}[e^{i\,\mathbf{p}\cdot\mathbf{r}} - (-)^{S+T}e^{-i\,\mathbf{p}\cdot\mathbf{r}}]\chi_{M_S}^S\,\eta_{M_T}^T, \tag{4.6}$$

where $\chi_{M_S}^S$ and $\eta_{M_T}^T$ are two-nucleon spin and isospin states, respectively, $\mathcal{Y}_{LSJ}^{M_J}$ are standard spin-angle functions,

$$Z_{LSM_S}^{JM_J}(\hat{\mathbf{p}}) \equiv \sum_{M_L}\langle LM_L, SM_S|JM_J\rangle Y_{LM_L}(\hat{\mathbf{p}}), \quad (4.7)$$

and $\langle LM_L, SM_S|JM_J\rangle$ are Clebsch-Gordan coefficients. Note that the wave function in Eq. (4.6) retains interaction effects only in channels with $J \leqslant J_{max}$ and reduces to plane waves for $J > J_{max}$.

When the Coulomb interaction is present, we use the method developed originally in Ref. [38], which allows us to solve the pp scattering problem in momentum space [39]. It consists essentially in separating the potential into short- and long-range parts v_S and v_L, where v_L only includes the Coulomb potential v_C, and v_S includes, in addition to v_C, the nuclear potential v. Then the standard momentum-space technique outlined earlier can be used to solve the problem with v_S, and the corresponding radial wave functions behave as

$$z_{S;L'L}^{JS1}(r;p) \simeq \frac{a_L}{2}\big[\delta_{L'L}h_L^{(2)}(pr) + h_{L'}^{(1)}(pr)S_{S;L'L}^{JS1}(p)\big], \quad (4.8)$$

where S_S^{JS1} is the S matrix in this case (with $T = 1$), and the a_L are normalization constants. The wave functions $z_{S;L'L}^{JS1}$ should match smoothly those relative to $v_S + v_L$, which behave asymptotically as

$$z_{L'L}^{JS1}(r;p) \simeq \tfrac{1}{2}\big[\delta_{L'L}\overline{h}_L^{(2)}(\xi, pr) + \overline{h}_{L'}^{(1)}(\xi, pr)S_{L'L}^{JS1}(p)\big], \quad (4.9)$$

where

$$\overline{h}_L^{(1,2)}(\xi, y) = [F_L(\xi; y) \mp G_L(\xi; y)]/y, \quad \xi = \alpha\,\mu/p, \tag{4.10}$$

and F_L and G_L are the regular and irregular Coulomb functions. Carrying out the matching for the functions and their first derivatives leads to a relation between S_S^{JS1} and S^{JS1} and a determination of the normalization constants [39]. Finally, pp scattering wave functions with incoming-wave boundary conditions are written as in Eq. (4.6) with $T, M_T = 1, 1$ and the replacement

$$z_{L'L}^{JS1*}(r;p) \longrightarrow e^{-i\,\sigma_L}z_{L'L}^{JS1*}(r;p), \tag{4.11}$$

where σ_L is the Coulomb phase shift,

$$\sigma_L = \arg[\Gamma(L+1+i\,\xi)]. \tag{4.12}$$

Hence, Coulomb interaction effects are retained only in channels with $J \leqslant J_{max}$ and are ignored in those with $J > J_{max}$.

B. The bound-state problem in momentum space

The deuteron wave function is written in r space as

$$\psi_M(\mathbf{r}) = \sum_{L=0,2} i^L u_L(r) \, \mathcal{Y}_{L11}^M(\hat{\mathbf{r}}) \, \eta_0^0, \qquad (4.13)$$

and the radial wave functions $u_L(r)$ $(L = 0, 2)$ follow from

$$u_L(r) = \frac{2}{\pi} \int_0^\infty \mathrm{d}p \, p^2 \, j_L(pr) \, \overline{u}_L(p). \qquad (4.14)$$

The p-space wave functions $\overline{u}_L(p)$ are obtained from solution of the homogeneous integral equations

$$\overline{u}_L(p) = \frac{1}{E_d - p^2/(2\mu)} \frac{2}{\pi} \int_0^\infty \mathrm{d}k \, k^2 \sum_{L'=0,2} v_{LL'}^{110}(p;k) \, \overline{u}_{L'}(k). \qquad (4.15)$$

Here, $v_{L'L}^{110}$ is the nuclear potential in the $JST = 110$ channel, and E_d is the deuteron energy ($E_d = -2.225$ MeV). We again note the unconventional phase i^L in Eq. (4.13).

C. Matrix elements, response functions, and cross sections

The deuteron wave function in Eq. (4.13) is written, for each spatial configuration $\mathbf{r}$, as a vector in the spin-isospin space of the two nucleons,

$$\psi_M(\mathbf{r}) = \sum_{n=1}^{8} \psi_M^{(n)}(\mathbf{r}) |n\rangle, \qquad (4.16)$$

where $|n\rangle = (p\uparrow)_1 (n\uparrow)_2, (n\uparrow)_1 (p\uparrow)_2, \ldots, (n\downarrow)_1 (p\downarrow)_2$ and $\psi_M^{(n)}$ are the components of ψ_M in this basis. In NC-induced processes, the scattering wave function in Eq. (4.6) is expanded on the same basis; however, in CC-induced processes the pp or nn scattering wave functions are expanded on the (spin-only) basis $|m\rangle = \uparrow\uparrow, \downarrow\uparrow, \uparrow\downarrow$, and $\downarrow\downarrow$ for pp or nn. Matrix elements of the weak-current operators are written schematically as

$$\langle f | O | d, M \rangle = \int \mathrm{d}\mathbf{r} \sum_{n',n} \psi_f^{(n')*}(\mathbf{r}) \, O_{n',n}(\mathbf{r}) \, \psi_M^{(n)}(\mathbf{r}), \qquad (4.17)$$

where the momentum- and energy-transfer dependence is understood. The spin-isospin algebra is performed exactly with techniques similar to those developed in Ref. [40], while the $\mathbf{r}$-space integrations are carried out efficiently by Gaussian quadratures. Note that no multipole expansion of the transition operators is required. When momentum operators are present, they are taken to act on the right (deuteron) wave function. For example, the one-body axial charge operator is written as

$$O(\mathbf{r}) \psi_M(\mathbf{r}) \longrightarrow -\frac{G_A(Q^2)}{4m} [e^{i\,\mathbf{q}\cdot\mathbf{r}/2} \, \boldsymbol{\sigma}_1 \cdot (-2i\boldsymbol{\nabla} + \mathbf{q}) \, \tau_{1,z}$$
$$+ 1 \rightleftharpoons 2] \psi_M(\mathbf{r}), \qquad (4.18)$$

and the derivatives are evaluated numerically as

$$\nabla_\alpha \psi_M(\mathbf{r}) \simeq \frac{\psi_M(\mathbf{r} + \delta \, \hat{\mathbf{e}}_\alpha) - \psi_M(\mathbf{r} - \delta \, \hat{\mathbf{e}}_\alpha)}{2\delta}, \qquad (4.19)$$

where $\hat{\mathbf{e}}_\alpha$ is a unit vector in the α direction, and δ is a small increment. Once the matrix elements have been computed,

response functions are evaluated (in the laboratory frame) via

$$R_{ab}(q, \omega) = \frac{1}{3} \sum_M \sum_{SM_S,T} \int \frac{\mathrm{d}\mathbf{p}}{(2\pi)^3} \frac{1}{2} \delta(\omega + m_d - E_+ - E_-)$$
$$\times f_{ab}^{SM_S, TM_T; M}(\mathbf{q}, \mathbf{p}), \qquad (4.20)$$

with

$$f_{ab}^{SM_S, TM_T; M}(\mathbf{q}, \mathbf{p}) = \langle \mathbf{q}, \mathbf{p}; SM_S, TM_T | O_a(\mathbf{q}, \omega) | d, M \rangle$$
$$\times \langle \mathbf{q}, \mathbf{p}; SM_S, TM_T | O_b(\mathbf{q}; \omega) | d, M \rangle^*, \qquad (4.21)$$

where $|\mathbf{q}, \mathbf{p}; SM_S, TM_T\rangle$ represents the final two-nucleon scattering state with total momentum $\mathbf{q}$ and relative momentum $\mathbf{p}$, m_d is the deuteron rest mass, and $E_\pm$ are the nucleons' energies in the final state,

$$E_\pm = \sqrt{(\mathbf{q}/2 \pm \mathbf{p})^2 + m^2}. \qquad (4.22)$$

The factor $1/2$ in Eq. (4.20) is to avoid double-counting the contribution of the final states (which are antisymmetrized), and the pair isospin T assumes the values $T = 0, 1$ with $M_T = 0$ for NC processes, and $T = 1$ with $M_T = 1$ or -1 for CC processes. The δ function is integrated out, and

$$R_{ab}(q, \omega) = \frac{1}{24\pi^2} \sum_M \sum_{SM_S,T} \int_{-1}^{+1} \mathrm{d}x \, p^2$$
$$\times \left| \frac{p + x\,q/2}{E_+} + \frac{p - x\,q/2}{E_-} \right|^{-1}$$
$$\times f_{ab}^{SM_S, TM_T; M}(q, p, x), \qquad (4.23)$$

where $x = \hat{\mathbf{q}} \cdot \hat{\mathbf{p}}$, and the magnitude p of the relative momentum is fixed by energy conservation. This magnitude depends on q, ω, and x. However, in order to reduce the computational effort, the scattering states entering the product of matrix elements f_{ab} are obtained at the energy

$$4(\overline{p}^2 + m^2) = (\omega + m_d)^2 - q^2, \qquad (4.24)$$

TABLE II. Total cross sections (in cm^2) for NC- and CC-induced processes on the deuteron as a function of the initial neutrino energy ϵ, obtained with the AV18 potential and the inclusion of one- and two-body terms in the weak current. The number in parentheses ("$-x$") denotes 10^{-x}; for instance, the entry 9.561(-44) stands for 9.561×10^{-44} cm^2.

ϵ (MeV)	ν_l-NC	$\overline{\nu}_l$-NC	ν_e-CC	$\overline{\nu}_e$-CC
5	9.561(-44)	9.363(-44)	3.427(-43)	2.831(-44)
10	1.104(-42)	1.053(-42)	2.680(-42)	1.242(-42)
20	6.965(-42)	6.285(-42)	1.547(-41)	9.562(-42)
30	1.833(-41)	1.568(-41)	4.058(-41)	2.508(-41)
40	3.555(-41)	2.885(-41)	7.995(-41)	4.685(-41)
50	5.892(-41)	4.546(-41)	1.348(-40)	7.403(-41)
60	8.839(-41)	6.495(-41)	2.338(-40)	1.057(-40)
70	1.240(-40)	8.699(-41)	2.949(-40)	1.409(-40)
80	1.657(-40)	1.111(-40)	4.036(-40)	1.790(-40)
90	2.131(-40)	1.369(-40)	5.320(-40)	2.191(-40)
100	2.657(-40)	1.640(-40)	6.631(-40)	2.606(-40)

TABLE III. Total cross sections (in cm^2) for NC-induced processes on the deuteron as a function of the initial neutrino energy ϵ, obtained with the AV18 potential and the inclusion of one-body (1) and (one + two)-body (1 + 2) terms in the weak current. Results corresponding to continuum final states (C) and plane-wave final states (PW) are listed.

ϵ (MeV)	$\nu_l(1,\mathrm{C})$	$\nu_l(1+2,\mathrm{C})$	$\nu_l(1,\mathrm{PW})$	$\nu_l(1+2,\mathrm{PW})$	$\bar{\nu}_l(1,\mathrm{C})$	$\bar{\nu}_l(1+2,\mathrm{C})$	$\bar{\nu}_l(1,\mathrm{PW})$	$\bar{\nu}_l(1+2,\mathrm{PW})$
100	2.577(−40)	2.657(−40)	2.469(−40)	2.510(−40)	1.604(−40)	1.640(−40)	1.607(−40)	1.619(−40)
150	5.720(−40)	5.935(−40)	5.626(−40)	5.752(−40)	3.003(−40)	3.075(−40)	3.096(−40)	3.124(−40)
200	9.435(−40)	9.846(−40)	9.384(−40)	9.650(−40)	4.345(−40)	4.460(−40)	4.526(−40)	4.576(−40)
250	1.324(−39)	1.389(−39)	1.324(−39)	1.369(−39)	5.531(−40)	5.695(−40)	5.778(−40)	5.858(−40)
300	1.683(−39)	1.772(−39)	1.689(−39)	1.754(−39)	6.546(−40)	6.762(−40)	6.842(−40)	6.962(−40)
350	2.003(−39)	2.116(−39)	2.014(−39)	2.101(−39)	7.420(−40)	7.687(−40)	7.752(−40)	7.917(−40)
400	2.279(−39)	2.414(−39)	2.295(−39)	2.403(−39)	8.186(−40)	8.504(−40)	8.545(−40)	8.760(−40)
450	2.509(−39)	2.664(−39)	2.531(−39)	2.660(−39)	8.856(−40)	9.221(−40)	9.255(−40)	9.520(−40)
500	2.703(−39)	2.874(−39)	2.727(−39)	2.874(−39)	9.503(−40)	9.916(−40)	9.906(−40)	1.023(−40)
550	2.861(−39)	3.046(−39)	2.888(−39)	3.051(−39)	1.010(−39)	1.056(−39)	1.052(−39)	1.089(−39)
600	2.989(−39)	3.185(−39)	3.019(−39)	3.196(−39)	1.068(−39)	1.118(−39)	1.110(−39)	1.153(−39)
650	3.093(−39)	3.299(−39)	3.125(−39)	3.315(−39)	1.124(−39)	1.178(−39)	1.166(−39)	1.214(−39)
700	3.176(−39)	3.390(−39)	3.210(−39)	3.411(−39)	1.178(−39)	1.237(−39)	1.221(−39)	1.275(−39)
750	3.243(−39)	3.463(−39)	3.278(−39)	3.489(−39)	1.232(−39)	1.295(−39)	1.275(−39)	1.333(−39)
800	3.297(−39)	3.522(−39)	3.333(−39)	3.552(−39)	1.284(−39)	1.352(−39)	1.327(−39)	1.391(−39)
850	3.340(−39)	3.570(−39)	3.377(−39)	3.603(−39)	1.337(−39)	1.408(−39)	1.379(−39)	1.448(−39)
900	3.374(−39)	3.608(−39)	3.412(−39)	3.644(−39)	1.388(−39)	1.463(−39)	1.430(−39)	1.504(−39)
950	3.403(−39)	3.639(−39)	3.440(−39)	3.678(−39)	1.440(−39)	1.518(−39)	1.481(−39)	1.559(−39)
1000	3.425(−39)	3.663(−39)	3.461(−39)	3.704(−39)	1.490(−39)	1.572(−39)	1.530(−39)	1.613(−39)

which only depends on q and ω. Finally, Gauss points ($\sim$50) are used to perform the x integration accurately. Extensive and independent tests of the computer programs have been completed successfully.

Total cross sections are obtained by direct integration of Eq. (2.3) by evaluating the differential cross sections on a grid of Gauss points in ϵ' (the lepton final energy) and θ (its scattering angle). There are kinematical constraints on the allowed values for ϵ' and θ, which follow from the requirement $\bar{p}^2 \geqslant 0$:

$$
\epsilon \sqrt{\epsilon'^2 - m_l^2} \cos\theta \geqslant (\epsilon + m_d)(\epsilon' - \bar{\epsilon}),
$$
$$
\bar{\epsilon} = \frac{m_d(\epsilon - \epsilon_{\mathrm{th}}) + m_l(m_l + 2\,m)}{\epsilon + m_d}, \tag{4.25}
$$

TABLE IV. Same as Table III, but for CC-induced processes.

ϵ (MeV)	$\bar{\nu}_e(1,\mathrm{C})$	$\bar{\nu}_e(1+2,\mathrm{C})$	$\bar{\nu}_e(1,\mathrm{PW})$	$\bar{\nu}_e(1+2,\mathrm{PW})$	$\nu_e(1,\mathrm{C})$	$\nu_e(1+2,\mathrm{C})$	$\nu_e(1,\mathrm{PW})$	$\nu_e(1+2,\mathrm{PW})$
100	2.567(−40)	2.606(−40)	2.362(−40)	2.370(−40)	6.424(−40)	6.631(−40)	5.908(−40)	6.023(−40)
150	4.688(−40)	4.751(−40)	4.487(−40)	4.491(−40)	1.516(−39)	1.574(−39)	1.440(−39)	1.477(−39)
200	6.736(−40)	6.830(−40)	6.555(−40)	6.568(−40)	2.605(−39)	2.719(−39)	2.525(−39)	2.603(−39)
250	8.677(−40)	8.822(−40)	8.520(−40)	8.567(−40)	3.775(−39)	3.958(−39)	3.699(−39)	3.833(−39)
300	1.059(−39)	1.082(−39)	1.044(−39)	1.056(−39)	4.928(−39)	5.186(−39)	4.854(−39)	5.052(−39)
350	1.254(−39)	1.286(−39)	1.239(−39)	1.261(−39)	5.981(−39)	6.315(−39)	5.923(−39)	6.189(−39)
400	1.455(−39)	1.499(−39)	1.441(−39)	1.475(−39)	6.920(−39)	7.320(−39)	6.876(−39)	7.210(−39)
450	1.663(−39)	1.722(−39)	1.650(−39)	1.698(−39)	7.778(−39)	8.248(−39)	7.704(−39)	8.102(−39)
500	1.879(−39)	1.952(−39)	1.865(−39)	1.930(−39)	8.524(−39)	9.053(−39)	8.410(−39)	8.868(−39)
550	2.100(−39)	2.189(−39)	2.087(−39)	2.169(−39)	9.064(−39)	9.636(−39)	9.005(−39)	9.519(−39)
600	2.323(−39)	2.428(−39)	2.309(−39)	2.410(−39)	9.556(−39)	1.017(−38)	9.504(−39)	1.007(−38)
650	2.548(−39)	2.671(−39)	2.537(−39)	2.656(−39)	9.966(−39)	1.062(−38)	9.920(−39)	1.053(−38)
700	2.777(−39)	2.916(−39)	2.766(−39)	2.905(−39)	1.031(−38)	1.098(−38)	1.027(−38)	1.091(−38)
750	3.005(−39)	3.161(−39)	2.995(−39)	3.152(−39)	1.059(−38)	1.129(−38)	1.055(−38)	1.124(−38)
800	3.232(−39)	3.403(−39)	3.223(−39)	3.399(−39)	1.082(−38)	1.154(−38)	1.079(−38)	1.150(−38)
850	3.456(−39)	3.645(−39)	3.448(−39)	3.643(−39)	1.101(−38)	1.176(−38)	1.099(−38)	1.173(−38)
900	3.678(−39)	3.882(−39)	3.671(−39)	3.885(−39)	1.118(−38)	1.193(−38)	1.116(−38)	1.192(−38)
950	3.896(−39)	4.116(−39)	3.890(−39)	4.122(−39)	1.131(−38)	1.208(−38)	1.129(−38)	1.208(−38)
1000	4.109(−39)	4.343(−39)	4.105(−39)	4.356(−39)	1.142(−38)	1.221(−38)	1.141(−38)	1.222(−38)
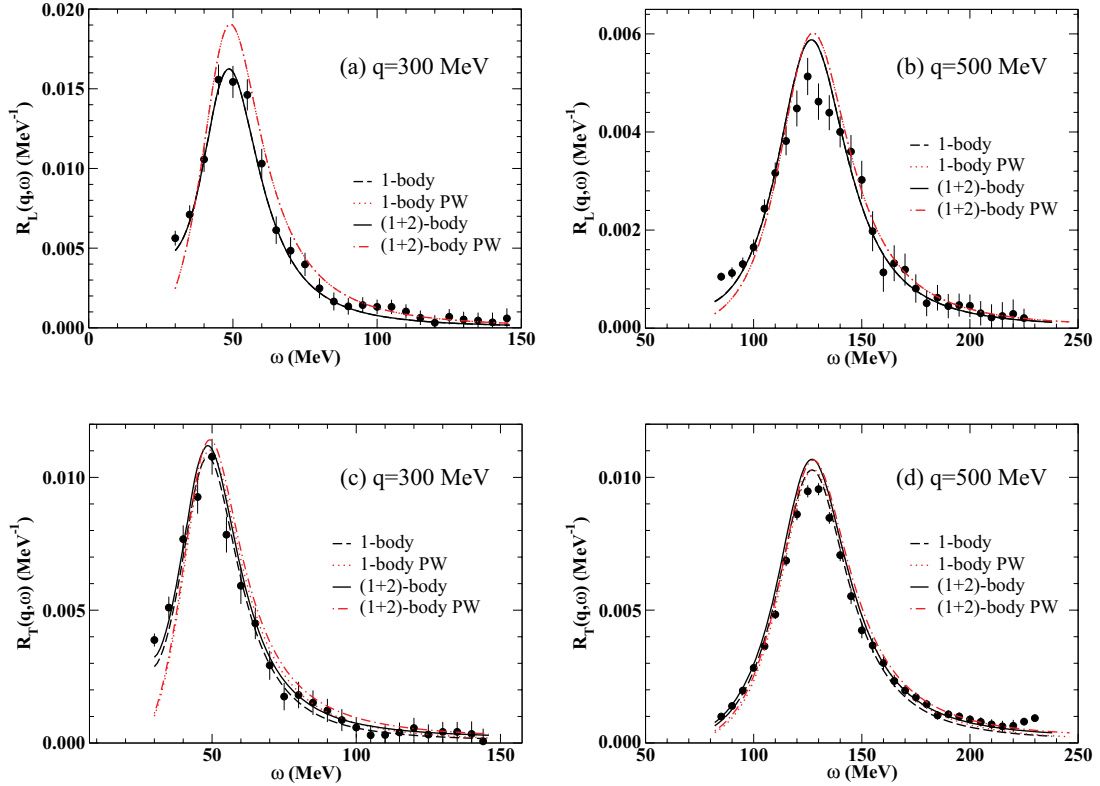
FIG. 1. (Color online) Electromagnetic responses: longitudinal at $q = 300$ MeV (a); longitudinal at $q = 500$ MeV (b): transverse at $q = 300$ MeV (c); transverse at $q = 500$ MeV (d). These are obtained with the AV18 potential and the inclusion of one-body (dashed line) and (one + two)-body (solid line) terms in the nuclear electromagnetic charge operator and are compared to data. Also shown are the results obtained with plane-wave (PW) final states.

where ϵ_{th} is the threshold energy for the initial neutrino ($\epsilon > \epsilon_{\mathrm{th}}$),

$$\epsilon_{\mathrm{th}} = \frac{(m_l + 2\,m)^2 - m_d^2}{2\,m_d}, \tag{4.26}$$

m_l is the rest mass of the final lepton ($m_l = 0$ in the NC case), and $m = (m_p + m_n)/2$ for NC reactions or $m = m_p$ (m_n) for charge-raising (charge-lowering) reactions. These kinematical constraints imply

$$m_l \leqslant \epsilon' \leqslant \epsilon'_- \quad \text{for} \quad -1 \leqslant \cos\theta \leqslant 0, \tag{4.27}$$

$$m_l \leqslant \epsilon' \leqslant \epsilon'_+ \quad \text{for} \quad 0 \leqslant \cos\theta \leqslant 1, \tag{4.28}$$

where the limits $\epsilon'_\pm$ are defined as

$$\epsilon'_\pm = \frac{\bar{\epsilon} \pm \sqrt{\bar{\epsilon}^2 - (1 - \beta^2 \cos^2\theta)(\bar{\epsilon}^2 + m_l^2 \beta^2 \cos^2\theta)}}{1 - \beta^2 \cos^2\theta},$$

$$\beta = \frac{1}{1 + m_d/\epsilon}. \tag{4.29}$$

In the case of NC reactions ($m_l = 0$), they are simply given by

$$0 \leqslant \epsilon' \leqslant \frac{\bar{\epsilon}}{1 - \beta\cos\theta} \quad \text{for} \quad -1 \leqslant \cos\theta \leqslant 1. \tag{4.30}$$

TABLE V. Total cross sections (in cm^2) for NC- and CC-induced processes on the deuteron obtained in Ref. [12] and in the present work at selected initial neutrino energies. Note that the values under the heading "this work" are slightly different from those reported in Table II, for the reasons explained in the text.

| | ϵ | | | | | |
| | 5 MeV | | 50 MeV | | 100 MeV | |
	Ref. [12]	This work	Ref. [12]	This work	Ref. [12]	This work
ν_l-NC	9.570(-44)	9.601(-44)	5.944(-41)	5.942(-41)	2.711(-40)	2.703(-40)
$\bar{\nu}_l$-NC	9.364(-44)	9.403(-44)	4.535(-41)	4.589(-41)	1.647(-40)	1.674(-40)
ν_e-CC	3.463(-43)	3.440(-43)	1.376(-40)	1.367(-40)	6.836(-40)	6.735(-40)
$\bar{\nu}_e$-CC	2.836(-44)	2.842(-44)	7.372(-41)	7.475(-41)	2.618(-40)	2.659(-40)
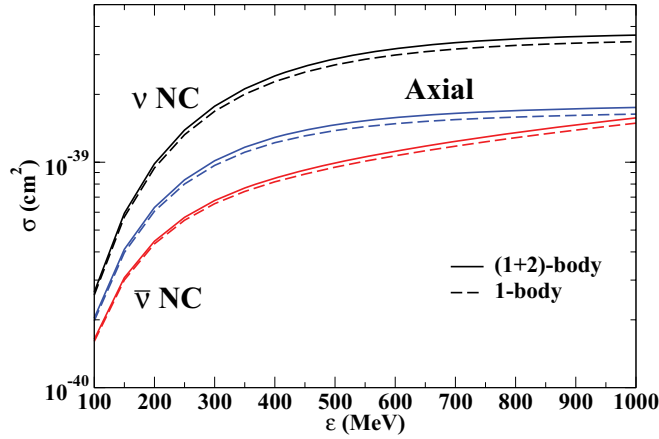
FIG. 2. (Color online) Total cross sections for NC-induced processes on the deuteron, obtained with the AV18 potential and the inclusion of one-body (dashed line) and (one + two)-body (solid line) terms in the weak current. Also shown are the total cross sections obtained by retaining only the axial piece of the weak current. See text for explanation.

V. RESULTS

Cross-section values obtained with the AV18 interaction and the one- and two-body terms in the electroweak current discussed in Sec. III are listed in Tables II–IV for initial neutrino energies in the range (5–1000) MeV. The two-body axial currents are those corresponding to set I in Table I. The two-nucleon (NN) scattering states are written as in Eq. (4.6): they include interaction effects in channels with $J \leqslant J_{max} = 5$ and reduce to spherical Bessel functions (i.e., plane waves) for $J > J_{max}$. The relative kinetic energy $T = 2 (\overline{p}^2 + m^2)^{1/2} - 2 m$, where $\overline{p}$ is defined in Eq. (4.24), changes over a wide range as the initial neutrino energy increases up to 1 GeV and the final lepton energy and scattering angle vary over the allowed kinematical regions: at $\epsilon = 50$ MeV, $0 \lesssim T \lesssim 48$ MeV; at
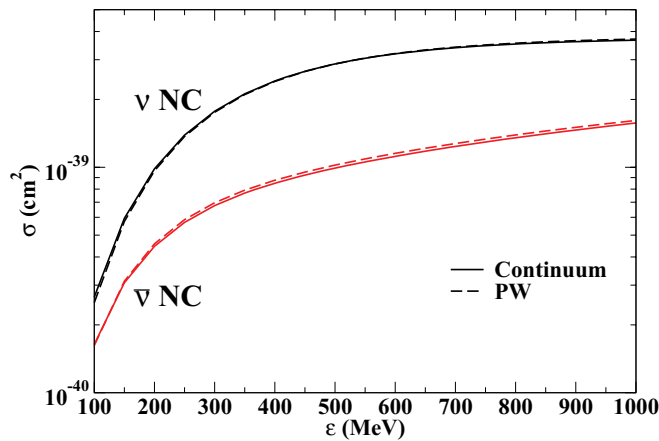
FIG. 3. (Color online) Total cross sections for NC-induced processes on the deuteron, obtained with the AV18 potential and the inclusion of (one + two)-body terms in the weak current. Also shown are the total cross sections obtained with plane-wave (PW) final states.
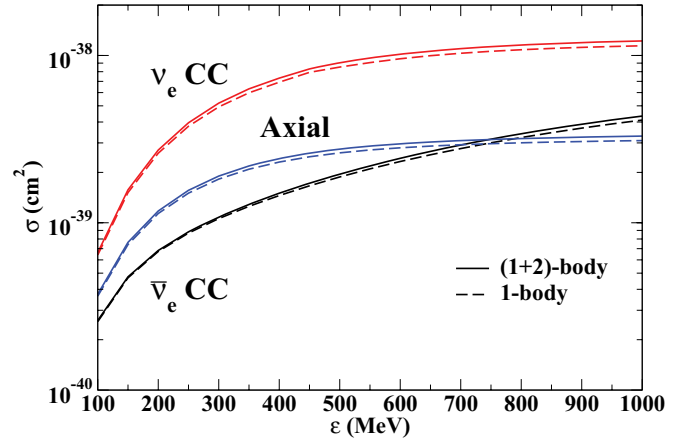
FIG. 4. (Color online) Same as Fig. 2, but for CC-induced processes on the deuteron.

$\epsilon = 500$ MeV, $0 \lesssim T \lesssim 445$ MeV; and at $\epsilon = 1000$ MeV, $0 \lesssim T \lesssim 819$ MeV. These relative energies (at the larger values of ϵ) are well beyond the range of applicability of all modern realistic interactions, which are typically constrained to fit NN scattering data up to pion production threshold ($T \simeq 150$ MeV). This is also the case for the AV18 of course, although it is known [41] that this interaction reproduces quite well phase shifts (at least in those channels where inelasticities are small) up to $T \lesssim 300$ MeV.

As an additional caveat, we note that the present theory cannot describe the inclusive cross section in the pion-production region, for example, the Δ-excitation peak region, as no mechanisms for (real) single- or multipion production are included in it. However, it does reproduce quite well the observed $d(e, e')$ inclusive cross section in the quasielastic peak region at intermediate values of the three-momentum transfer. This is illustrated in Figs. 1(a)–1(d), where the longitudinal and transverse response functions R_L and R_T obtained at Bates [42] by Rosenbluth separation of (e, e') data at momentum transfers of 300 and 500 MeV are compared with theory. In these figures, we show separately the
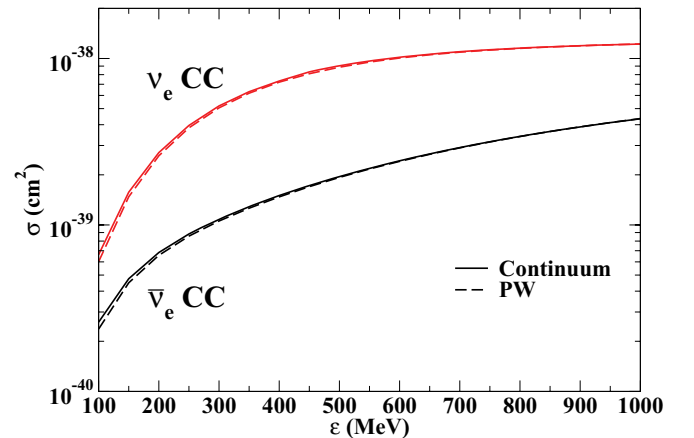
FIG. 5. (Color online) Same as Fig. 3, but for CC-induced processes on the deuteron.

TABLE VI. Total cross sections (in cm^2) for NC- and CC-induced processes on the deuteron at selected initial neutrino energies, obtained with the AV18 potential and the inclusion of one-body and set I or set II two-body terms in the weak current.

ϵ (MeV)	ν_l-NC		$\overline{\nu}_l$-NC		ν_e-CC		$\overline{\nu}_e$-CC	
	Set I	Set II	Set I	Set II	Set I	Set II	Set I	Set II
5	9.561(-44)	9.541(-44)	9.363(-44)	9.344(-44)	3.427(-43)	3.421(-43)	2.831(-44)	2.826(-44)
50	5.892(-41)	5.873(-41)	4.546(-41)	4.530(-41)	1.348(-40)	1.353(-40)	7.403(-41)	7.380(-41)
100	2.657(-40)	2.652(-40)	1.640(-40)	1.636(-40)	6.631(-40)	6.621(-40)	2.606(-40)	2.600(-40)

response functions calculated with an electromagnetic current including one-body only and (one + two)-body terms, as well as those obtained by replacing the fully interacting NN states of Eq. (4.6) with plane waves (curves labeled PW). Two-body terms in R_L give negligible contributions; those in R_T lead to an increase in the transverse strength over the whole quasielastic region, which amounts to a few percent at the top of the peak but becomes sizable (relative to the one-body response) as the energy transfer ω increases well beyond the quasielastic peak energy $\omega_{\mathrm{qe}} = (q^2 + m^2)^{1/2} - m$. At these momentum transfers, the quasielastic and Δ peaks in R_T, the latter at $\omega_\Delta = (q^2 + m_\Delta^2)^{1/2} - m$ ($m_\Delta = 1232$ MeV), are well separated; note, however, the rise seen in the data at $q = 500$ MeV and the highest ω's, presumably owing to (transverse) strength creeping in from the Δ-peak region. Interaction effects in the NN continuum states are important, particularly at low momentum transfers and/or for energy transfers close to the threshold for deuteron breakup. However, at the larger q values plane-wave states provide response functions in the quasielastic region, which are fairly close to those predicted by the exact scattering states. Finally, we note that at $q = 500$ MeV and quasielastic energies, theory overpredicts the measured longitudinal response. As a consequence, the total integrated longitudinal strength—the Coulomb sum rule—obtained from these data [40] is smaller than calculated. On the other hand, there is excellent agreement between the theoretical and the measured Coulomb sum rules at $q = 300$ (and 400) MeV [40].

In Table II the columns labeled ν_l-NC and $\overline{\nu}_l$-NC refer to the NC-induced reactions in Eq. (2.1), those labeled ν_e-CC and $\overline{\nu}_e$-CC refer to CC-induced reactions in Eq. (2.2), and the initial neutrino energy is between 5 MeV (close to threshold) and 100 MeV. In this energy range the cross sections change rapidly, by 3–4 orders of magnitude, and interaction effects in the final scattering states are important. Two-body terms in the vector and axial pieces of the weak current increase

the one-body cross section typically by 2–3% for both NC- and CC-induced reactions, in agreement with the results in Ref. [12].

There are differences between the present calculations and those of Nakamura *et al.* [12]—mostly having to do with the model for the weak current—which, however, lead to only small numerical differences in the predicted cross-section values, as shown below. As remarked in Sec. III B, the authors of that work ignore the relativistic corrections proportional $1/m^2$ in the one-body axial current (3.9) and use a different short-range parametrization for the two-body vector and axial currents than adopted here. In addition, the cutoff masses entering the nucleon form factors have values slightly different from those listed in Sec. III A. In order to have a more meaningful comparison with the results of that work, we carried out a calculation of the NC- and CC-induced cross sections at three representative initial neutrino energies, in which we removed the relativistic correction in the one-body axial current and changed the cutoff mass values in the nucleon form factors so as to match those used in Ref. [12]. Inspection of Table V shows that the two calculations are typically within less than 1% of each other. This level of agreement should be viewed as satisfactory, given the different ways in which the two calculations are carried out in practice. The authors of Ref. [12] rely on a multipole expansion of the cross section, whereas we compute the matrix elements entering the various response functions by direct numerical integrations, which avoid the need for introducing (cumbersome) multipole expansions of the weak transition operators. Of course, the present calculations are computationally intensive: evaluation of the NC cross sections requires about 40 min per neutrino energy on 512 processors and similar times for each of the two CC cross sections.

The calculated cross sections for NC- and CC-induced reactions are listed, respectively, in Tables III and IV for incident

TABLE VII. Total cross sections (in cm^2) for NC-induced processes on the deuteron at selected initial neutrino energies, obtained with the AV18 or CD-Bonn (CDB) potentials and the inclusion of one-body terms (1) only and both one- and two-body terms (1 + 2) in the weak current.

ϵ (MeV)	ν_l-NC				$\overline{\nu}_l$-NC			
	AV18(1)	CDB(1)	AV18(1 + 2)	CDB(1 + 2)	AV18(1)	CDB(1)	AV18(1 + 2)	CDB(1 + 2)
50	5.747(-41)	5.791(-40)	5.892(-41)	5.847(-40)	4.449(-41)	4.484(-40)	4.546(-41)	4.519(-40)
100	2.577(-40)	2.597(-40)	2.657(-40)	2.638(-40)	1.604(-40)	1.617(-40)	1.640(-40)	1.633(-40)
500	2.703(-39)	2.715(-39)	2.874(-39)	2.858(-39)	9.503(-40)	9.553(-40)	9.916(-40)	9.895(-40)
1000	3.425(-39)	3.442(-39)	3.663(-39)	3.659(-39)	1.490(-39)	1.496(-39)	1.572(-39)	1.572(-39)
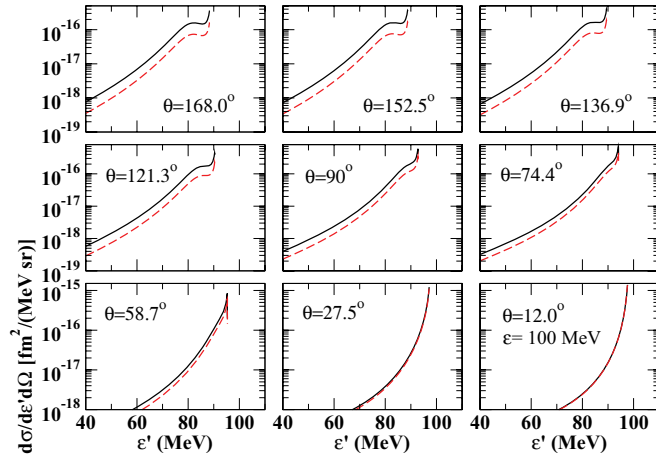
FIG. 6. (Color online) Differential cross section for NC-induced processes on the deuteron, obtained with the AV18 potential and the inclusion of one- and two-body terms in the nuclear weak current, as a function of the final lepton energy. The incident neutrino energy is 100 MeV. The final lepton angle is indicated in each panel. The solid (black) curve represents neutrino-induced processes; the dashed (red) curve, antineutrino-induced processes.

neutrino energies between 100 and 1000 MeV. The columns labeled (1,C) and (1 + 2,C) [(1,PW) and (1 + 2,PW)] list results obtained by including fully interacting (plane-wave) NN final states and one-body only or (one + two)-body terms in the weak current. These results are also displayed in Figs. 2–5. The two-body contributions are small, less than 10% over the whole energy range. Interaction effects in the final states are found to be even smaller, which suggests that realistic estimates for these cross sections on the deuteron (and possibly nuclei with $A > 2$) at high energies may be obtained by approximating the final nuclear states by plane waves, i.e., by employing the nucleon momentum distribution in the deuteron (or the spectral function in $A > 2$ nuclei). Finally, in Figs. 2 and 4 we also show the results obtained by including only the axial piece in the weak current. In this case, the interference response function R_{xy} vanishes, and consequently, the ν_l and $\bar{\nu}_l$ cross sections are the same. For CC-induced reactions, owing to the charge de-
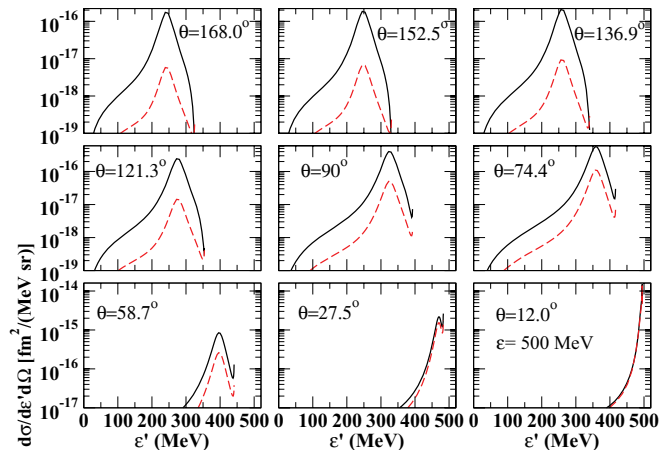
FIG. 7. (Color online) Same as Fig. 6, but the incident neutrino energy is 500 MeV.
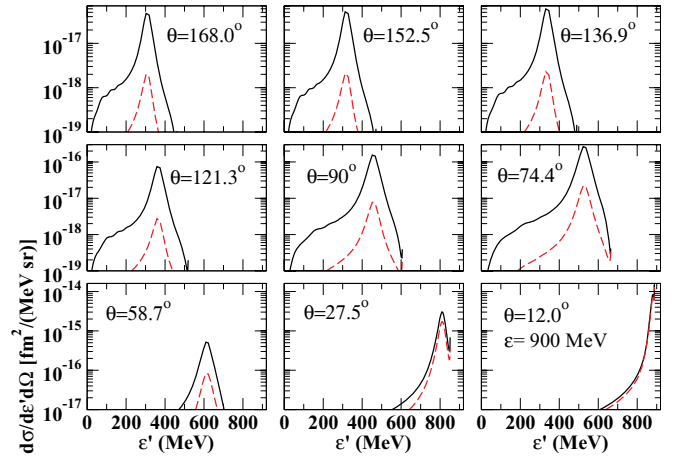
FIG. 8. (Color online) Same as Fig. 6, but the incident neutrino energy is 900 MeV.

pendence of the NN final state (pp or nn) the neutrino-induced CC reaction has a slightly larger cross section (a few percent) even with only the axial piece in the weak current. We display the axial contribution in the antineutrino-induced CC reactions in Fig. 4. Axial contributions are larger than vector at low energies, $\lesssim$400–500 MeV, but become smaller than vector at higher energies.

The sensitivity of the results on the model used for the two-body axial current (set I or set II) and NN potential (AV18 or CD-Bonn) is investigated, respectively, in Tables VI and VII. In both cases, the model dependence is found to be negligible. The two-body vector currents are taken from the AV18, and therefore their short-range behavior is not consistent with the CD-Bonn interaction. This inconsistency, though, is of little numerical import. Furthermore, because interaction effects in the two-nucleon continuum appear to be negligible for neutrino energies $\gtrsim$100 MeV, the agreement of the calculated cross
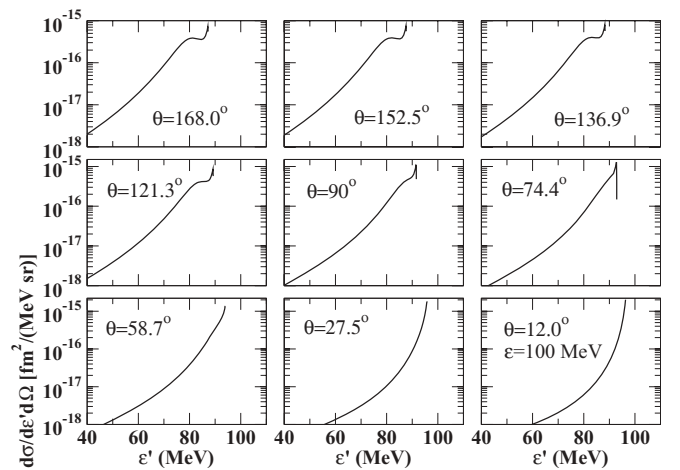
FIG. 9. Differential cross section for electron antineutrino-induced CC processes on the deuteron, obtained with the AV18 potential and the inclusion of one- and two-body terms in the nuclear weak current, as a function of the final lepton energy. The incident antineutrino energy is 100 MeV. The final lepton angle is indicated in each panel.
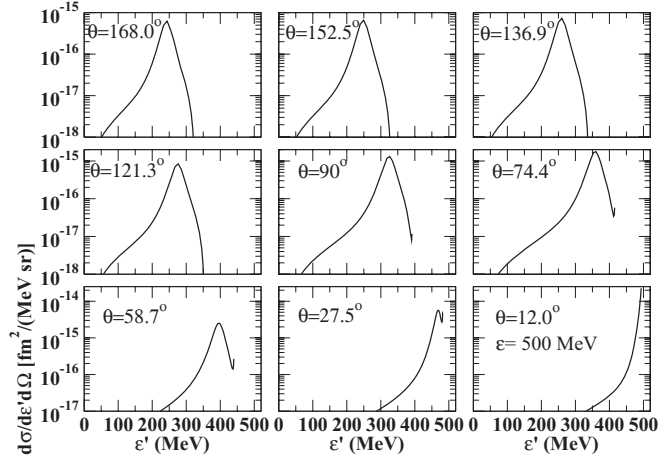
FIG. 10. Same as Fig. 9, but the incident neutrino energy is 500 MeV.

sections between the AV18 and CD-Bonn merely reflects the fact that the momentum distributions predicted by these two potential models are very close to each other for relative momenta $\lesssim 400$ MeV.

In Figs. 6–14 we show the differential cross sections for NC- and CC-induced reactions as a function of the final lepton energy ϵ' and scattering angle θ at three incident neutrino energies, $\epsilon = 100$, 500, and 900 MeV. The quasielastic peak is located at a final energy $\epsilon'_{\rm qe}$ given by

$$\epsilon'_{\rm qe} = \frac{\epsilon}{1 + (2\,\epsilon/m)\sin^2\theta/2}, \qquad (5.1)$$

where we have neglected the lepton mass in the case of CC processes. Therefore as θ changes from the backward to the forward hemisphere, the quasielastic peak moves to the right, i.e., towards higher and higher energies. Indeed, at forward angles it merges with the threshold peak owing to the quasibound $^1S_0$ state. The latter peak is very pronounced at low ϵ but becomes more and more suppressed by the form factor $\sim \langle {}^1{\rm S}_0|j_0(q\,r/2)|d\rangle$ as ϵ increases.
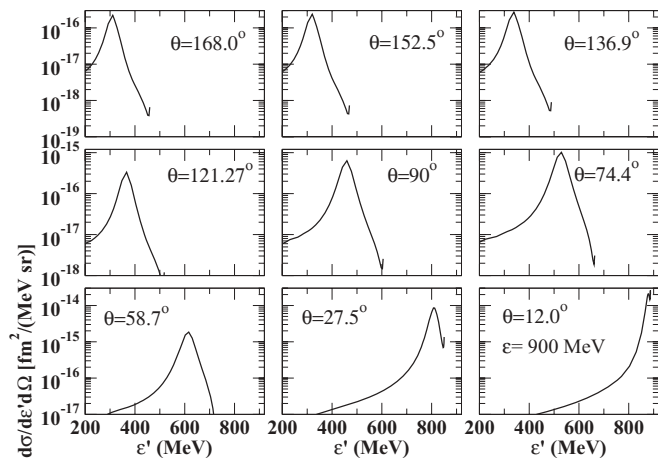
FIG. 11. Same as Fig. 9, but the incident neutrino energy is 900 MeV.
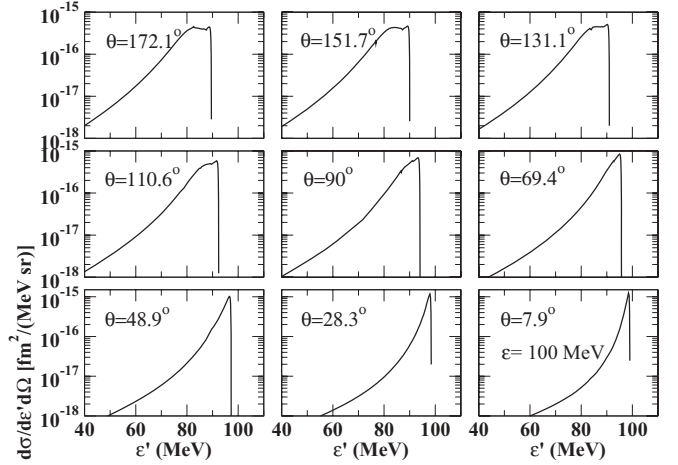
FIG. 12. Differential cross section for electron neutrino-induced CC processes on the deuteron, obtained with the AV18 potential and the inclusion of one- and two-body terms in the nuclear weak current, as a function of the final lepton energy. The incident neutrino energy is 100 MeV. The final lepton angle is indicated in each panel.

Finally, it is interesting to compare the results above with those obtained in a naive model, in which the deuteron is taken to consist of a free proton and neutron initially at rest. The laboratory-frame cross sections of NC-induced processes on the nucleon, and of CC-induced processes $n(\nu_e, e^-)p$ and $p(\overline{\nu}_e, e^+)n$ in the limit in which the final electron/positron mass and proton-neutron mass difference are neglected, read [43]

$$\left(\frac{d\sigma}{d\epsilon' d\Omega}\right)_{\nu/\overline{\nu}}^{\rm NC/CC} = \frac{G^2\,m^2}{8\pi^2}\left(\frac{\epsilon'}{\epsilon}\right)^2 \delta(\epsilon' - \epsilon'_{\rm qe})\Bigg[A^{\rm NC/CC}$$
$$\mp \frac{s-u}{m^2}B^{\rm NC/CC} + \frac{(s-u)^2}{m^4}C^{\rm NC/CC}\Bigg],$$
$$(5.2)$$

where $G = G_F$ or $G_F\cos\theta_C$ for NC or CC, the minus (plus) sign in the second term is relative to the ν $(\overline{\nu})$ initiated reactions,
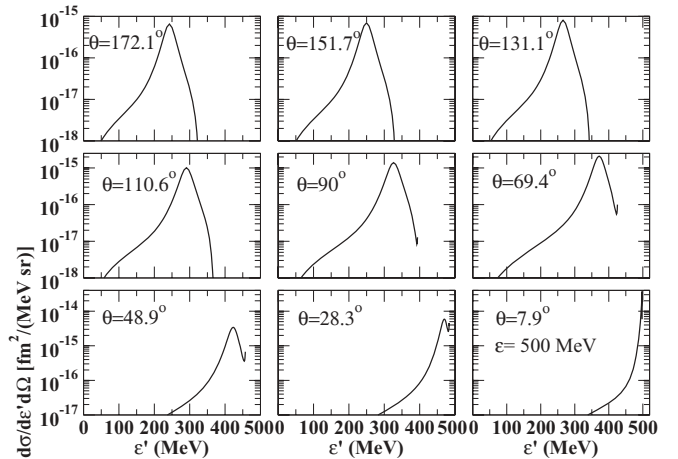
FIG. 13. Same as Fig. 12, but the incident neutrino energy is 500 MeV.
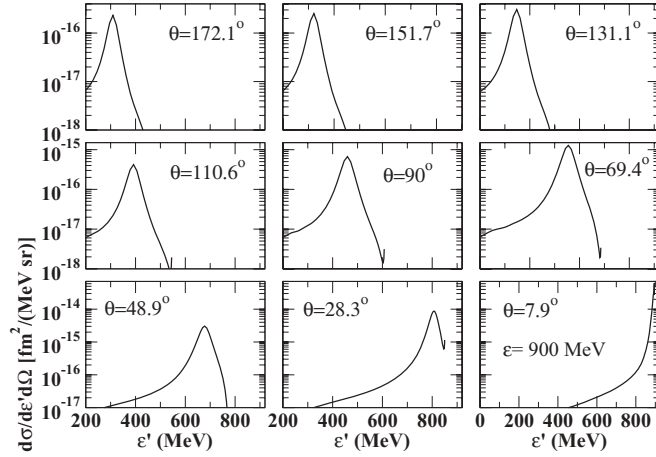
FIG. 14. Same as Fig. 12, but the incident neutrino energy is 900 MeV.

ϵ'_{qe} has been defined in Eq. (5.1), and $s - u = 4m\epsilon - Q^2$ with $Q^2 = 4\epsilon\epsilon' \sin^2\theta/2$. The structure functions $A(Q^2)$, $B(Q^2)$, and $C(Q^2)$ for both NC and CC are given in terms of nucleon form factors in Appendix B.

In the naive model, the ν- and $\bar\nu$-deuteron NC cross sections are simply given by the sum of the corresponding proton and neutron (NC) cross sections, while the ν-deuteron ($\bar\nu$-deuteron) CC cross section is identified with the $n(\nu_e, e^-)p$ [$p(\bar\nu_e, e^+)n$] cross section. The "model" differential cross sections as a function of the final lepton scattering angle (after integrating out the energy-conserving δ function) are illustrated in Fig. 15 at three incident energies ($\epsilon = 100$, 500, and 900 MeV). The ν and $\bar\nu$ cross sections are about the same at forward angles, for which Q^2 is small; at backward angles, as ϵ and Q^2 increase, they both decrease owing to the fall-off in the form factors. However, this fall-off is much more pronounced (orders of magnitude) for the $\bar\nu$ than for the ν cross sections. (At the low energy of 100 MeV, the form factors do not change much with angle and the variation with angle in the differential cross section is mild; still, it decreases more in the $\bar\nu$ than in the ν channel.) These features are reflected in the deuteron cross
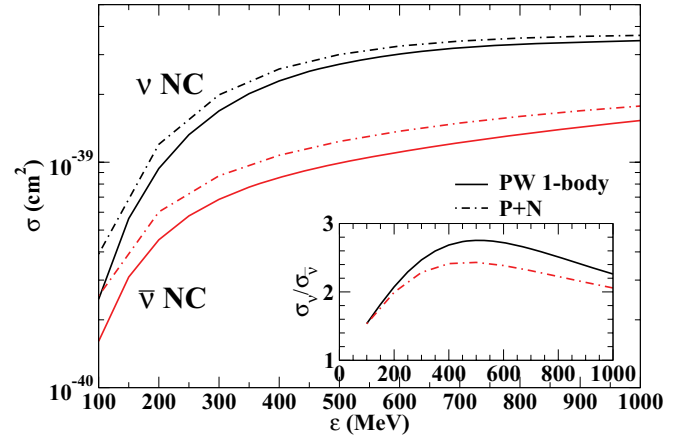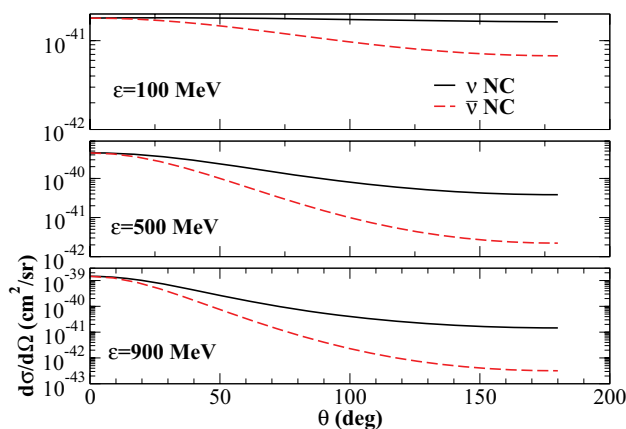
FIG. 16. (Color online) The "model" (P + N) NC cross sections for neutrino and antineutrino are compared with plane-wave one-body (PW 1-body) results; see the text for explanation. Inset: Ratio of neutrino NC to antineutrino NC cross section.

sections displayed in Figs. 6–14 (incidentally, in each panel of these figures the "model" cross sections would be represented by a δ function located at ϵ'_{qe}, corresponding to the energy of the quasielastic peak).

In order to illustrate nuclear correlation effects in the initial deuteron state, we compare the "model" ν and $\bar\nu$ NC cross sections with the plane-wave one-body results, shown in Fig. 16, for which we use the physical deuteron state, plane waves for the two-nucleon continuum states, and one-body currents. In both ν and $\bar\nu$ NC reactions, inclusion of nuclear correlations in the initial state reduces the cross sections from the naive model. In fact, a similar reduction in cross section (owing to nuclear correlations) at about nuclear density for uniform nuclear matter has been noticed, for example, in Refs. [44,45]. However, these correlations increase the ratio of ν to $\bar\nu$ NC cross sections, as shown in the inset in Fig. 16. Similar effects are also found in the ν and $\bar\nu$ CC reactions at low neutrino energies, as shown in Fig. 17. At higher energies, nuclear correlations hardly affect these cross sections, and the
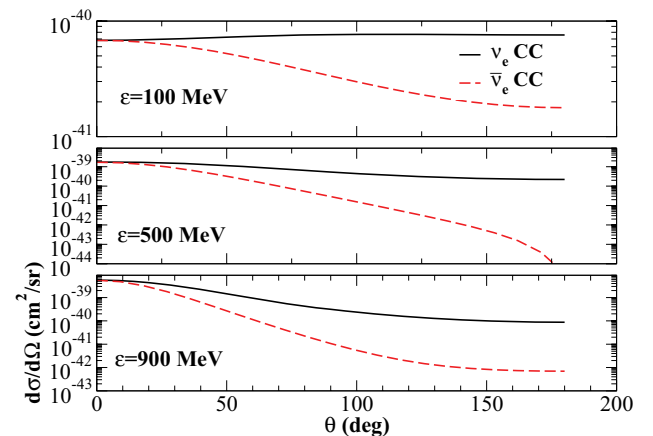
FIG. 15. (Color online) The "model" NC (left) and CC (right) differential cross sections for neutrino (solid lines) and antineutrino (dashed lines) energies of 100, 500, and 900 MeV, as functions of the final lepton scattering angle.
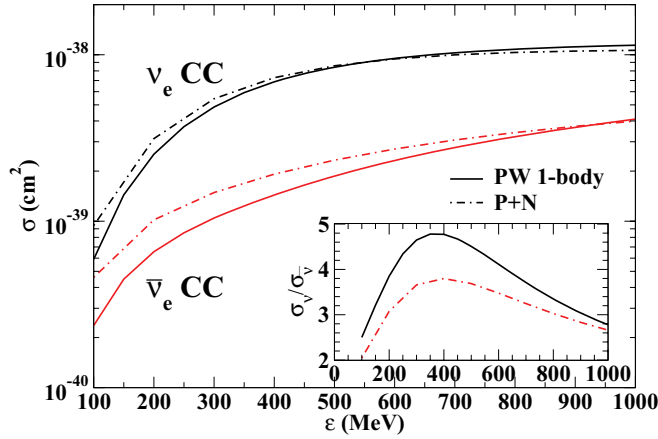
FIG. 17. (Color online) Same as Fig. 16, but for CC cross sections.

naive and realistic models are in better agreement with each other. The ratio of ν to $\bar{\nu}$ CC cross sections is also increased owing to nuclear correlations (see inset in Fig. 17). This fact may have interesting implications for long-baseline neutrino experiments aimed at extracting CP violating signals from the detection of differences in the neutrino and antineutrino channels.

VI. CONCLUSIONS AND OUTLOOK

In this work, we have studied inclusive neutrino scattering on the deuteron up to neutrino energies of 1 GeV, by using a realistic description of two-nucleon interactions and weak currents. Two-body terms in the latter increase the calculated cross sections with one-body currents by less than 10% over the whole energy region for both NC- and CC-induced processes. Interaction effects in the two-nucleon continuum final state are found to be negligible for neutrino energies $\gtrsim 500$ MeV. This suggests that fairly realistic estimates for these cross sections in light nuclei (and at relatively high neutrino energies) may be obtained in calculations based on the plane-wave impulse approximation. Even calculations in this limit, however, cannot presently be carried out, as they require knowledge of nuclear spectral functions over a wide range of missing momenta and energies, and these are not yet available in light nuclei. Nuclear correlation effects in the initial deuteron state are found to be important. They reduce the ν and, to a larger extent, $\bar{\nu}$ cross sections over the whole range of energies studied in this work and, therefore, significantly increase the ν to $\bar{\nu}$ cross-section ratio for both NC and CC reactions. In the present work the pion-production channels are not included. Experimentally they produce distinctive final states and make important contributions to total neutrino cross sections above pion-production threshold. It would be interesting to include these channels in future.

It should be possible to use quantum Monte Carlo methods [15] to study neutrino response functions, and associated sum rules, in light nuclei within the same (realistic) dynamical framework adopted here. Indeed, "exact" calculations of this type [46] led to a quantitatively accurate description of the quasielastic electromagnetic response functions measured in

$A = 3$ and 4 nuclei. In particular, they showed that the charge-exchange character of the nucleon-nucleon interaction leads to shifts of longitudinal and transverse strength at higher excitation energies, thus providing a quenching of the response in the quasielastic peak region. This mechanism, however, is more than offset in the transverse channel by two-body currents, in particular, those associated with pion exchange, and hence the response is enhanced over the entire quasielastic spectrum. It will be interesting to see the extent to which these considerations remain valid in the weak sector probed in neutrino scattering and will possibly provide an explanation for the observed anomaly in the ^{12}C data.

APPENDIX A

The cross section for CC processes at low incident neutrino energies in which the lepton mass cannot be neglected reads

$$\left(\frac{d\sigma}{d\epsilon' d\Omega}\right)_{\nu/\bar{\nu}} = \frac{G^2}{8\pi^2} \frac{k'}{\epsilon} F(Z, k')[v_{00} R_{00} + v_{zz} R_{zz} - v_{0z} R_{0z} + v_{xx+yy} R_{xx+yy} \mp v_{xy} R_{xy}], \quad (A1)$$

where the kinematical factors are given by

$$v_{00} = 2\epsilon\epsilon' \left(1 + \frac{k'}{\epsilon'}\cos\theta\right), \quad (A2)$$

$$v_{zz} = \frac{\omega^2}{q^2}\left[m_l^2 + 2\epsilon\epsilon'\left(1 + \frac{k'}{\epsilon'}\cos\theta\right)\right] + \frac{m_l^2}{q^2}\left[m_l^2 + 2\omega(\epsilon + \epsilon') + q^2\right], \quad (A3)$$

$$v_{0z} = \frac{\omega}{q}\left[m_l^2 + 2\epsilon\epsilon'\left(1 + \frac{k'}{\epsilon'}\cos\theta\right)\right] + m_l^2\frac{\epsilon+\epsilon'}{q}, \quad (A4)$$

$$v_{xx+yy} = Q^2 + \frac{Q^2}{2q^2}\left[m_l^2 + 2\epsilon\epsilon'\left(1 + \frac{k'}{\epsilon'}\cos\theta\right)\right] - \frac{m_l^2}{q^2}\left[\frac{m_l^2}{2} + \omega(\epsilon' + \epsilon)\right], \quad (A5)$$

$$v_{xy} = Q^2\frac{\epsilon+\epsilon'}{q} - m_l^2\frac{\omega}{q}, \quad (A6)$$

m_l is the final lepton mass, and the response functions are defined as in Eqs. (2.5)–(2.9). Note that

$$\epsilon + \epsilon' = \sqrt{2m_l^2 + (\mathbf{k} + \mathbf{k}')^2 + Q^2}, \quad (A7)$$

and the cross section above is easily shown to reduce to Eq. (2.3) in the limit $m_l = 0$ and $Q^2 = 4\epsilon\epsilon'\sin^2\theta/2$.

APPENDIX B

In this Appendix, the structure functions entering NC- and CC-induced processes on the nucleon are expressed in terms of (nucleon) form factors. In the NC case, they read

$$A^{NC} = 4\,\eta\left[(1+\eta)\left(\overline{F}_A^N\right)^2 - (1-\eta)\left(\overline{F}_1^N\right)^2\right.$$
$$\left. + \eta\,(1-\eta)\left(\overline{F}_2^N\right)^2 + 4\,\eta\,\overline{F}_1^N\overline{F}_2^N\right], \quad (B1)$$

$$B^{NC} = 4\,\eta\,\overline{F}_A^N\left(\overline{F}_1^N + \overline{F}_2^N\right), \quad (B2)$$

$$C^{NC} = \tfrac{1}{4}\left[\left(\overline{F}_A^N\right)^2 + \left(\overline{F}_1^N\right)^2 + \eta\left(\overline{F}_2^N\right)^2\right], \quad (B3)$$

and $\eta = Q^2/(4\,m^2)$. The nucleon form factors $\overline{F}_i^N$ and $\overline{F}_A^N$ for $N = p$ or n are defined as

$$2\,\overline{F}_i^{p/n} = (1 - 4\,\sin^2\theta_W)\,F_i^{p/n} - F_i^{n/p}, \quad (B4)$$

$$2\,\overline{F}_A^{p/n} = \mp\,G_A, \quad (B5)$$

where the proton and neutron electromagnetic form factors are, respectively, $F_i^p = (F_i^S + F_i^V)/2$ and $F_i^n = (F_i^S - F_i^V)/2$, with $F_i^{S/V}$ defined in Eqs. (3.43) and (3.44) and the axial form factor G_A (with $-$ for p and $+$ for n) as defined in Eq. (3.12). In the limit in which the final lepton mass and proton-neutron mass difference are both neglected, the relations for the A, B, and C structure functions remain valid for the CC case, provided

$$\overline{F}_i^N \longrightarrow F_i^V, \quad \overline{F}_A^N \longrightarrow G_A. \quad (B6)$$

[1] A. A. Aguilar-Arevalo *et al.*, Phys. Rev. Lett. **100**, 032301 (2008).

[2] A. V. Butkevich, Phys. Rev. C **82**, 055501 (2010).

[3] O. Benhar, P. Coletti, and D. Meloni, Phys. Rev. Lett. **105**, 132301 (2010).

[4] C. Juszczak, J. T. Sobczyk, and J. Zmuda, Phys. Rev. C **82**, 045502 (2010).

[5] E. Amaldi, S. Fubini, and G. Furlan, *Electroproduction at Low Energy and Hadron Form Factors, Springer Tracts in Modern Physics No. 83* (Springer-Verlag, Berlin, 1979), p. 1.

[6] N. J. Baker *et al.*, Phys. Rev. D **23**, 2499 (1981); K. L. Miller *et al.*, *ibid.* **26**, 537 (1982).

[7] T. Kitagaki *et al.*, Phys. Rev. D **28**, 436 (1983).

[8] L. A. Ahrens *et al.*, Phys. Rev. D **35**, 785 (1987).

[9] G. Garvey (private communication).

[10] K. Kubodera and S. Nozawa, Int. J. Mod. Phys. E **3**, 101 (1994).

[11] S. Nakamura, T. Sato, V. Gudkov, and K. Kubodera, Phys. Rev. C **63**, 034617 (2001).

[12] S. Nakamura *et al.*, Nucl. Phys. A **707**, 561 (2002); [http://www.physics.sc.edu/gudkov/NU-D-NSGK/].

[13] Q. R. Ahmad *et al.* (SNO Collaboration), Phys. Rev. Lett. **89**, 011301 (2002); S. N. Ahmed *et al.* (SNO Collaboration), *ibid.* **92**, 181301 (2004).

[14] J. N. Bahcall and M. H. Pinsonneault, Phys. Rev. Lett. **92**, 121301 (2004).

[15] J. Carlson and R. Schiavilla, Phys. Rev. Lett. **68**, 3682 (1992); Phys. Rev. C **49**, R2880 (1994).

[16] I. S. Towner and J. C. Hardy, in *Physics Beyond the Standard Model*, edited by P. Herczeg, C. M. Hoffman, and H. V. Klapdor-Kleingrothaus (World Scientific, Singapore, 1999), p. 338.

[17] K. Nakamura *et al.* (Particle Data Group), J. Phys. G **37**, 075021 (2010).

[18] I. S. Towner, Phys. Rev. C **58**, 1288 (1998).

[19] A. Kurylov, M. J. Ramsey-Musolf, and P. Vogel, Phys. Rev. C **65**, 055501 (2002); **67**, 035502 (2003).

[20] D. T. Spayde *et al.* (SAMPLE Collaboration), Phys. Rev. Lett. **84**, 1106 (2000); (SAMPLE Collaboration), Phys. Lett. B **583**, 79 (2004); E. J. Beise, M. L. Pitt, and D. T. Spayde, Prog. Part. Nucl. Phys. **54**, 289 (2005).

[21] Z. Ahmed *et al.* (HAPPEX Collaboration), Phys. Rev. Lett. **108**, 102001 (2012); K. A. Aniol *et al.* (HAPPEX Collaboration), Phys. Rev. C **69**, 065501 (2004); A. Acha *et al.* (HAPPEX Collaboration), Phys. Rev. Lett. **98**, 032301 (2007).

[22] C. E. Hyde-Wright and K. de Jager, Annu. Rev. Nucl. Part. Sci. **54**, 217 (2004).

[23] T. Gorringe and H. W. Fearing, Rev. Mod. Phys. **76**, 31 (2004); P. Kammel and K. Kubodera, Annu. Rev. Nucl. Part. Sci. **60**, 327 (2010).

[24] A. Czarnecki, W. J. Marciano, and A. Sirlin, Phys. Rev. Lett. **99**, 032003 (2007).

[25] L. E. Marcucci, A. Kievsky, S. Rosati, R. Schiavilla, and M. Viviani, Phys. Rev. Lett. **108**, 052502 (2012); L. E. Marcucci, M. Piarulli, M. Viviani, L. Girlanda, A. Kievsky, S. Rosati, and R. Schiavilla, Phys. Rev. C **83**, 014002 (2011).

[26] V. A. Andreev *et al.*, Phys. Rev. Lett. **99**, 032002 (2007).

[27] P. Ackerbauer *et al.*, Phys. Lett. B **417**, 224 (1998).

[28] V. Bernard, N. Kaiser, and U.-G. Meissner, Phys. Rev. D **50**, 6899 (1994); N. Kaiser, Phys. Rev. C **67**, 027002 (2003).

[29] J. Carlson and R. Schiavilla, Rev. Mod. Phys. **70**, 743 (1998).

[30] L. E. Marcucci, R. Schiavilla, M. Viviani, A. Kievsky, S. Rosati, and J. F. Beacom, Phys. Rev. C **63**, 015801 (2000).

[31] L. E. Marcucci, M. Viviani, R. Schiavilla, A. Kievsky, and S. Rosati, Phys. Rev. C **72**, 014001 (2005).

[32] C. E. Carlson, Phys. Rev. D **34**, 2704 (1986).

[33] J. Carlson, V. R. Pandharipande, and R. Schiavilla, in *Modern Topics in Electron Scattering*, edited by B. Frois and I. Sick (World Scientific, Singapore, 1991), p. 177.

[34] R. Machleidt, Phys. Rev. C **63**, 024001 (2001).

[35] K. Kubodera, J. Delorme, and M. Rho, Phys. Rev. Lett. **40**, 755 (1978).

[36] R. Schiavilla, J. Carlson, and M. Paris, Phys. Rev. C **70**, 044007 (2004).

[37] W. Glöckle, *The Quantum Mechanical Few-Body Problem* (Springer-Verlag, Berlin, 1983).

[38] C. M. Vincent and S. C. Phatak, Phys. Rev. C **10**, 391 (1974).

[39] J. Carlson, R. Schiavilla, V. R. Brown, and B. F. Gibson, Phys. Rev. C **65**, 035502 (2002).

[40] R. Schiavilla, V. R. Pandharipande, and A. Fabrocini, Phys. Rev. **40**, 1484 (1989).

[41] R. B. Wiringa, www.phy.anl.gov/theory/research/av18/.

[42] S. A. Dytman *et al.*, Phys. Rev. C **38**, 800 (1988).

[43] A. W. Thomas and W. Weise, *The Structure of the Nucleon* (Wiley-VCH Verlag, Berlin, 2001).

[44] C. J. Horowitz and K. Wehrberger, Nucl. Phys. A **531**, 665 (1991).

[45] S. Reddy, M. Prakash, J. M. Lattimer, and J. A. Pons, Phys. Rev. C **59**, 2888 (1999).

[46] J. Carlson, J. Jourdan, R. Schiavilla, and I. Sick, Phys. Rev. C **65**, 024002 (2002).